ACCSCIENCE PUBLISHING

International Journal of Bioprinting

RESEARCH ARTICLE

Three-dimensional-printed collagen scaffold with limbal stem cells derived from adipose-derived mesenchymal stem cells for the treatment of limbal stem cell deficiency

Martha Stokking[1†], Marta Cadenas-Martín[1†], Ana I. Martín-González[1], Alba Fernández-Ferrer[1], Francisco Arnalich-Montiel[2], and Maria P. De Miguel[1*]

[1]Cell Engineering Laboratory, La Paz University Hospital Health Research Institute (IdiPAZ), Madrid, Spain

[2]Ophthalmology Department, Ramón y Cajal Institute for Biohealth Research (IRYCIS), Ramón y Cajal University Hospital, Madrid, Spain

[†]These authors contributed equally to this work.

***Corresponding author:**
Maria P. De Miguel
(mmiguelgonzalez@salud.madrid.org)

Citation: Stokking M, Cadenas-Martin M, Martín-González AI, Fernández-Ferrer A, Arnalich-Montiel F, De Miguel MP. Three-dimensional-printed collagen scaffold with limbal stem cells derived from adipose-derived mesenchymal stem cells for the treatment of limbal stem cell deficiency. *Int J Bioprint*. 2025;11(6):407-429. doi: 10.36922/IJB025290293

Received: July 18, 2025
1st revised: August 27, 2025
2nd revised: September 5, 2025
Accepted: September 8, 2025
Published online: September 8, 2025

Abstract

When limbal stem cell deficiency (LSCD) is partial, the standard treatment involves covering the corneal surface with amniotic membrane (AM), which supports the proliferation of the remaining limbal stem cells (LSCs). In cases of complete LSCD, the most common treatment is cultured limbal epithelial transplantation (CLET), although there is a risk of rejection. Studies have shown that mesenchymal stem cell transplantation is equally safe and effective as CLET. Recent research has demonstrated successful differentiation of adipose-derived adult mesenchymal stem cells (ADSCs) into LSCs. Combining AM transplantation with LSCs improves treatment efficacy. However, a limitation of AM use is donor variability and the associated risk of immune rejection. We propose the use of 3D-printed collagen as a scaffold seeded with LSCs derived from ADSCs for the treatment of LSCD in a rat model. The 3D-printed collagen scaffolds exhibited good transparency. *In vitro* differentiation of ADSCs into LSCs showed morphological changes that were more pronounced and occurred more rapidly on 3D-printed collagen. Among the tested substrates, 3D-printed collagen was the most efficient for differentiation, yielding the highest expression of LSC-specific markers (p63α and BMI-1) and the corneal epithelial marker (SSEA-4). LSCs differentiated in either AM or 3D-printed collagen I scaffolds were transplanted into a rat model of LSCD and compared with the standard, cell-free AM treatment. In all treatment groups, the induced epithelial wound was closed; however, integration of the 3D-printed collagen scaffold was statistically superior to that of AM. However, markers for different corneal structures (PAS, BMI-1, p63α, and cytokeratins 12 and 13) indicated that the generated epithelium was conjunctival rather than corneal, suggesting that the contribution of ADSC-derived LSCs was insufficient for complete corneal re-epithelization.

Keywords: Amniotic membrane; Bioprinting; Cornea; Limbal stem cell deficiency; Mesenchymal stem cells; Regenerative medicine; Tissue engineering; Vision loss

1. Introduction

The cornea is a transparent, avascular structure located at the front of the eye. Histologically, it is composed of the following three main cellular layers: epithelium, stroma, and endothelium. The most superficial layer is the epithelium, a stratified layer that accounts for approximately 10% of the total corneal thickness. It serves as a protective barrier against mechanical injury and external biological agents. The corneal stroma comprises about 90% of the total thickness and is composed primarily of an organized extracellular matrix rich in collagen and proteoglycans. This layer provides the cornea with strength, morphology, and transparency.[1] The endothelium is a single layer of cells whose primary function is to regulate corneal hydration through a pump-leak mechanism, thereby maintaining corneal transparency.[2] Each of these layers can be selectively replaced through either full-thickness (penetrating) or lamellar keratoplasty techniques, depending on the depth and extent of the corneal pathology.[3] However, these keratoplasty techniques typically involve only the central portion of the cornea and, therefore, do not address limbal stem cell deficiency (LSCD), which affects the peripheral cornea and requires a distinct therapeutic approach.

Damage to the corneal epithelium is usually repaired through self-regeneration, driven by a specialized population of corneal epithelial stem cells located at the limbus, known as limbal stem cells (LSCs).[4] These LSCs typically undergo asymmetric division, producing one daughter cell that remains in the niche to preserve the stem cell pool and another that becomes a transient amplifying cell (TAC). TACs proliferate rapidly and differentiate into the various functional cells of the corneal epithelium, collectively known as corneal epithelial cells.[5] Epithelial repair follows a coordinated centripetal and upward growth pattern.[6]

The differentiation and maturation of the corneal epithelium are linked to the expression of cytokeratin 12 (CK-12), a type of intermediate filament essential for epithelial integrity,[7] which is expressed in all cell layers of the differentiated and stratified epithelium.[8] Stage-specific embryonic antigen-4 (SSEA-4) is a well-established marker for human embryonic stem cells. High levels of SSEA-4 expression have been observed in differentiated corneal epithelial cells as well as in the limbal epithelium.[9]

Unlike the corneal epithelium, no definitive marker has yet been established for LSCs, although several candidates have been proposed. One such candidate is the transcription factor p63α, which is expressed in progenitor cells within the basal layer of the limbal epithelium. Another relevant factor is BMI-1, a transcription factor associated with stem cell self-renewal, which has been identified in the human limbus.[10] Cytokeratin 19 (CK-19) has also emerged as a potential marker.[11]

Destruction or dysfunction of LSCs or their niche leads to LSCD.[12] In this condition, the loss of LSCs impairs the regenerative capacity of the corneal epithelium, allowing the conjunctival epithelium—a non-keratinized stratified squamous epithelium containing mucin (MUC)-secreting goblet cells—to invade the corneal surface. This process, known as conjunctivalization, compromises corneal transparency and promotes neovascularization. As a result, LSCD can lead to chronic ocular surface inflammation, persistent pain, and severe vision loss or blindness in advanced cases. Characteristic markers of the invading conjunctival epithelium include MUC and cytokeratin 13 (CK-13), the latter being expressed in all conjunctival epithelial cells.[13]

When LSCD is partial, one of the most commonly employed treatments is the application of amniotic membrane (AM) to cover the corneal surface. AM serves as a biological bandage that protects the damaged area from mechanical stress, promotes epithelial healing, reduces inflammation and pain, and facilitates the proliferation of the remaining LSCs.

In cases of total LSCD, if the disease is unilateral, several autologous approaches are available, such as conjunctival limbal autograft, which involves transplanting two relatively large limbal-conjunctival grafts from the healthy contralateral eye to the affected eye. An alternative, cultured limbal epithelial transplantation (CLET), requires only a small limbal biopsy, which is expanded *in vitro* and then transplanted to the damaged eye.[14] In bilateral LSCD, where no autologous donor tissue is available, treatment options include allogeneic CLET or keratolimbal allograft. These approaches require systemic immunosuppression, which increases the risk of patient morbidity.[15]

The rising number of bilateral LSCD cases has led to an increased reliance on allogeneic LSCs, which inherently carry the risk of immune rejection and necessitate long-term immunosuppressive therapy. To overcome these limitations, numerous research groups have explored the use of autologous stem cells of extraocular origin as an alternative source for ocular surface regeneration.

The use of mesenchymal stem cells (MSCs) has gained significant momentum in recent years.[15] Among these, bone marrow-derived MSCs have been extensively studied for ocular surface regeneration, showing promising results. However, adipose-derived stem cells (ADSCs) offer key practical advantages as follows: they are more readily accessible, cost-effective, and less invasive to obtain, which has led to their increasing popularity in translational

research.[16] At the clinical level, Calonge *et al.*[17] provided compelling evidence that MSC transplantation is as safe and effective as CLET for the treatment of LSCD.

More recently, our group and collaborators have shown that ADSCs can be successfully differentiated into LSC-like phenotypes, expressing key LSC markers.[18,19] Notably, using an LSC-specific induction medium, ADSCs achieved structural epithelial regeneration, further supporting their potential as an autologous cell source for ocular surface reconstruction.[16,19]

With respect to the cell carrier, the most widely used scaffold in clinical practice is the AM.[20] AM is a biologically active, avascular tissue. This collagen-rich matrix mimics the biochemical properties of the corneal and scleral stroma, facilitating cell migration, differentiation, and inhibition of apoptosis.[21] AM's biocompatibility and low immunogenicity make it practical and convenient for clinical use. However, in cases of total LSCD, AM transplantation alone is insufficient to restore a functional epithelium.[22] Combining AM with LSCs has shown improved therapeutic outcomes,[6] and more recently, AM seeded with MSCs has demonstrated the ability to restore a corneal epithelial phenotype in LSCD models.[16,19,23]

Despite its advantages, AM has several limitations, including donor variability, which can increase the risk of immunologic rejection in allogeneic settings. In addition, its scarcity and the complexity of procurement, processing, and storage contribute to significant costs and limit its widespread availability. Due to these limitations, alternative scaffolds are being actively investigated to support, or even stimulate, corneal epithelial regeneration prior to implantation on the damaged ocular surface. Among the biomaterials explored are fibrin, chitosan, and silk fibroin—materials that are biocompatible, mechanically resilient, and easy to handle. However, their clinical application may be hindered by immune rejection or suboptimal biomechanical properties, such as excessive rigidity, fragility, or insufficient tensile strength.[24]

Collagen-based scaffolds have emerged as a highly promising option due to their structural similarity to native corneal stroma and excellent biocompatibility. In parallel, advances in three-dimensional (3D) bioprinting have enabled the creation of complex, cell-compatible constructs using bioinks—formulations that combine living cells with biological materials.[25] The use of 3D-printing techniques to replicate complex patterns found in biological tissues is an emerging field in tissue engineering. Among these, extrusion-based bioprinting is particularly prominent due to its versatility and its ability to use a wide range of bioinks with varying viscosities. This technique uses pneumatic or mechanical forces for continuous layer-by-layer deposition. While pneumatic systems provide better control over bioink viscosities, they may cause cell membrane disruption due to pressure fluctuations. Conversely, mechanical systems offer precise control but introduce higher shear stress, which can affect cell viability. Optimizing critical parameters such as shear stress, nozzle diameter, and material crosslinking is essential for balancing cell viability with shape fidelity.[26] The combination of high speed and the ability to utilize highly viscous bioinks makes extrusion-based bioprinting particularly suitable for fabricating anatomically compliant constructs. Jetting-based bioprinting, in contrast, employs a drop-on-demand mechanism to deposit bioink droplets at pre-defined positions, enabling precise cell placement and enhanced cell–cell interactions. This technique includes several modalities, such as inkjet-based, electrohydrodynamic jet-based, laser-induced forward transfer-based bioprinting, and others. However, the jetting itself is governed by the surface tension and viscosity of the bioink, which restricts printability and limits the fabrication of large, anatomically complex constructs. Vat photopolymerization-based bioprinting stands out for its high resolution, making it ideal for fabricating intricate surface topographies. This technique utilizes selective light irradiation to induce localized curing of liquid biomaterials contained within a vat. Variants such as stereolithography, digital light processing, two-photon polymerization, and volumetric printing further expand its capabilities (for a comprehensive review, see Ng *et al.*[27]).

In this study, we propose the use of mechanically driven extrusion-based 3D-printed scaffolds, as this printing method allows for the use of highly concentrated and viscous collagen bioinks in continuous deposition layers, enabling control over the construct's shape. In addition, the constructs were colonized with adipose-derived stem cell–derived limbal stem cells (ADSC-LSCs) for the treatment of total LSCD in a rat model, as a step toward the development of fully autologous, bioengineered ocular surface reconstruction strategies.

2. Materials and methods

2.1. Scaffolds

2.1.1. Preparation of human amniotic membrane

A total of 64 cm^2 of human AM unsuitable for transplantation was obtained from a 37-year-old human donor via the Barcelona Blood and Tissue Bank. The sample was anonymized by the Barcelona Biobank, as stipulated by the Organic Law on Data Protection, and was accompanied by a serological analysis report showing negative for human immunodeficiency virus (HIV), hepatitis A virus (HAV), hepatitis B virus (HBV), hepatitis

C virus (HCV), human T-cell lymphotropic virus (HTLV), dengue virus, and syphilis. The sample was washed four times for 15 min with PBS to remove the glycerol in which it had been preserved, scraped on both sides to remove the epithelium, and cut into 6 mm diameter circles.

2.1.2. Three-dimensional bioprinting

Sheets of rat collagen I were obtained by 3D printing at the Cell Engineering Laboratory of the La Paz Health University Hospital Research Institute (IdiPAZ).[28] For the 3D printing, the Regemat® V1 mechanical extrusion printer (Regemat®, Spain) was used together with Regemat 3D Designer software (Regemat®, Spain), which enabled adjustment of the object geometry and configuration of printing parameters. A nozzle diameter of 580 μm was selected. Collagen bioink (Cellink®, Sweden) was neutralized to pH 7 and printed at a concentration of 8 mg/mL, with 9 μg/mL of proteoglycans (glycosaminoglycans) derived from goat cornea (R&D Systems, USA). The 3D-printed scaffolds were designed as flat cylindrical shapes with a diameter of 6 mm using an STL format. To obtain a thickness of approximately 100 μm, two layers were printed in a diagonal pattern oriented at 90° relative to each other. The printed cylinders underwent two post-printing curation steps: first, a gelation step involving incubation in a carbon dioxide (CO_2) cell culture incubator at 37°C for a minimum of 2 h (longer periods showed no added benefit); and second, a controlled dehydration step, in which the gelled samples were incubated in a 40% humidity-controlled chamber at 37°C for 1 week. This final step could be performed in a humidity-controlled environmental chamber (Thermo Fisher Scientific, USA) or chemically, by adding the saturated potassium carbonate (Sigma, USA) in a sealed glass desiccator (Sigma, USA). These curation steps ensured transparency and tensile strength rheological characteristics similar to AM (see Section 3). As the cornea is avascular, no vascularization strategies were employed.

2.1.3. Macroscopic characterization of the scaffolds

Optical coherence tomography was performed on both the AM and 3D-printed scaffolds to determine their thickness. In addition, graft transparency was assessed, following standard ophthalmological procedures, by placing AM and 3D-printed constructs on a black background and a back-lit chart composed of parallel black lines over a white background, in order to compare light transmittance and refraction, as described in previous studies.[29] This assessment was conducted by an ophthalmologist (FA-M) in a blinded fashion. Tensile strength was evaluated subjectively by the same ophthalmologist, also in a blinded manner, by placing sutures on two sides of the AM or 3D-printed scaffolds.

2.2. Mesenchymal stem cell isolation and culture

The cells used in this study were obtained through the isolation of human tissues via procedures approved by the Institutional Review Board of IdiPAZ (protocol code PI308) and deposited in the La Paz University Hospital Biobank. Ophthalmic cells were obtained under the approval of the Institutional Review Board of the Ramón y Cajal University Hospital (protocol code 305/11), or from commercial cell lines (ATCC, USA). All adipose tissue donations were collected with prior written informed consent from the donors, in line with the World Medical Association Declaration of Helsinki (2000) and the Organic Law on Data Protection, which guarantees donor anonymity. Each sample was subjected to serological analysis prior to processing to rule out active infection by HIV, HAV, HBV, HCV, HTLV, dengue virus, and syphilis, in compliance with the official state guidelines for the use of human cells and tissues for experimental purposes (Royal Decree 09/2014; July 4, 2014). No test for SARS-CoV-2 was performed, as all donations predated the COVID-19 pandemic.

Human adipose-derived mesenchymal stem cells (hADSCs) were extracted from the lipoaspirates of six female donors aged 37–55, with body mass indexes ranging from 26.4 to 31.8 kg/m^2, who had undergone elective liposuction. All donors were healthy and were not receiving any drug therapy, except for one who was being treated with fluoxetine for depression. The protocol already established by Zuk *et al.*[30] was followed, as previous studies by our laboratory demonstrated its effectiveness in isolating multipotent hADSCs capable of differentiating into multiple cell lineages. All cells were maintained in culture until reaching sub-confluence (80–90%) in their corresponding medium at 37°C with 5% CO_2, with medium changes three times per week. Subsequently, the cells were cryopreserved in liquid nitrogen using complete medium supplemented with 10% dimethyl sulfoxide (DMSO; EMSURE®, Abbott Laboratories, USA) for subsequent use in the various experiments.

2.3. Human adipose-derived mesenchymal stem cell differentiation into limbal stem cells

The hADSCs were differentiated into LSCs according to a previously published protocol.[18] Briefly, hADSC-derived limbal cells were differentiated for 7 days in an ectodermal induction medium of Dulbecco's Modified Eagle Medium (DMEM; Gibco, USA) with: GlutaMax (2 mM; Gibco, USA); sodium pyruvate (1 mM; Gibco™, USA); 15% fetal bovine serum (FBS; Gibco™); 1% penicillin/streptomycin (P/S) (Gibco™); 10 μM SB505124 (a transforming growth factor beta-pathway inhibitor; Merck KGaA, Germany); 10 μM IWP2 (a Wnt pathway inhibitor, Merck KGaA); and 50 ng/mL fibroblast growth factor 2 (ORF Genetics,

Iceland).[31] The second differentiation step lasted 10 days and used a corneal epithelial cell differentiation medium based on that of Casaroli-Marano *et al.*[32] named SHEM. This medium consisted of DMEM/Ham F12 (1:2) supplemented with: GlutaMax (2 mM); sodium pyruvate (1 mM; Gibco™); 2% FBS (Gibco™); 1% P/S (Gibco™); 5 μg/mL insulin (Humalog®, USA); 10 ng/mL human epidermal growth factor (Peprotech, USA); 0.18 mM adenine (Merck KGaA); 0.4 μg/mL hydrocortisone (Merck KGaA); 2 nM 3,30,5-triiodo-L-thyronine (T3) (Merck KGaA); 0.5% DMSO (EMSURE®); supplemented with 4 nM pigment epithelium-derived factor (PEDF; Peprotech); and 20 ng/mL keratinocyte growth factor (KGF; Peprotech).

Three different substrates were used: standard culture plastic, AM, and 3D-printed collagen I, each coated with 0.75 μg/cm^2 of vitronectin (Gibco™) to improve cell adhesion and differentiation efficiency.

2.4. Morphometric analysis of differentiation and kinetics

Differentiation kinetics were analyzed to morphological changes in the cells. The performance of the three different substrates during differentiation was evaluated by measuring the length and number of hADSCs before differentiation, 7 days after the first differentiation step, and 9 days after the second differentiation step. Measurements were taken using ImageJ software (version 1.51a, NIH, USA) from microscopic images of the cell cultures, following the method described by Cadenas-Martín *et al.*[18]

2.5. Immunofluorescence

Given that no specific marker exists for LSCs, while several are associated with the corneal limbal niche, we evaluated the differentiation efficiency of ADSC-LSCs cultured on plastic, 3D-printed collagen, and AM (all coated with vitronectin), by detecting the colocalization of nuclear p63α (1:100; 4892, Cell Signaling Technology Inc., USA) and BMI-1 (1:60; sc-390443, Santa Cruz Biotechnology, USA) markers, along with the cytoplasmic embryonic stem cell marker SSEA-4 (1:50/1:100; MAB1435, R&D Systems). For positive controls, the HaCat cell line was used for p63α and BMI-1, and the NTERA cell line for SSEA-4. For negative controls, the primary antibodies were omitted.

Quantitative data on marker positivity were obtained by calculating the ratio of positive to negative cells in 30 random fields at 630× magnification using a confocal microscope (DMI 4000 B, Leica, Germany).

2.6. *In vivo* studies

The animal studies complied with European Union regulations on vertebrate animal experimentation and were carried out in accordance with the 3Rs principle (replacement, reduction, and refinement), as stipulated in Royal Decree 53/2013 of February 1, 2013, on the protection of animals used for scientific purposes, and in accordance with the guidelines of the Association for Research in Vision and Ophthalmology. All procedures were performed by certified personnel authorized to conduct animal experimentation and approved by the Animal Welfare Committee of IdiPAZ, under the Regional Ministry of Environment, Agriculture, and the Interior of the Community of Madrid (code PROEX: 347.1/21). Animals were housed at the Experimental Surgery Service animal facility of IdiPAZ, Madrid (Registration Number: 280790001941).

2.6.1. Animal model and surgical procedures

Twenty-four female Sprague Dawley rats weighing 220–380 g were used to test the biosafety and efficacy of hADSC-LSCs on AM and 3D-printed collagen to repair corneal epithelium damage following LSC obliteration. The rats were randomly assigned to three groups (n=8 per group): control group with cell-free AM; experimental group 1 with 1×10^5 LSCs on AM; and experimental group 2 with 1×10^5 LSCs on 3D-printed collagen.

In the surgical procedure, a 4-min chemical burn was induced on the cornea of the right eye using heptanol, under anesthesia, according to a previously published protocol.[16] This was followed by mechanical removal of the remaining corneal epithelium and limbal region using an AlgerBrush II BR-2 1 mm (Eickemeyer, Germany). All rats received a retro-orbital injection of 40 mg/mL triamcinolone acetonide (Kenacort®, Bristol Myers Squibb Company, USA) for local immunosuppression. Subsequently, the animals were transplanted with one of the following: cell-free AM, AM with ADSC-LSCs, or 3D-printed collagen with ADSC-LSCs. A drop of fibrin glue (Tisseel, Baxter International Inc., USA) was applied beneath the scaffold to promote adhesion. Then, a 5.5 mm diameter ACLAR® (chlorotrifluoroethylene, OcuScience®, USA) contact lens was placed over the graft to prevent graft detachment and reduce pain. To prevent infection, Tobradex (Novartis, Switzerland) was applied, and the eyelid was closed with tarsorrhaphy using two 5/0 Vicryl stitches (Ethicon Inc., USA) to prevent self-inflicted trauma. Postoperative care included: tramadol (25 mg/kg; Grünenthal GmbH, Germany) subcutaneously once daily for 1 week, and one drop of Tobradex (Novartis) every 12 h. The animals were monitored for 10 days, until full reepithelialization was observed.

Out of the 24 rats used in the study, only half (n = 12) were suitable for final analysis. Eight rats died before the end of the study due to complications related to analgesia, not the surgical procedure. Four rats were excluded due to tissue processing issues—corneal epithelium was either

folded, absent, or the scaffold (AM or 3D-printed collagen) was missing from the paraffin block. Therefore, the final analysis included: three rats treated with cell-free-AM, five rats treated with LSC-AM, and four rats treated with LSC-3D-printed collagen.

2.6.2. Macroscopic study

The progression of re-epithelization was assessed using fluorescein staining (Bausch&Lomb, USA) and ultraviolet lamp photography of the treated eyes at the end of the 10-day experimental period.

2.6.3. Histopathology

Ten days after surgery, the rats were euthanized. The eyes were enucleated—right eyes (treated) and left eyes (untreated) in the case of negative controls. Corneas were fixed in 10% buffered formalin (VWR, USA), embedded in paraffin blocks, and sectioned at a thickness of 7 µm using a Leica RM2255 microtome. Sections were stained with hematoxylin-eosin or periodic acid–Schiff (PAS) stain and observed under an Olympus BX41 light microscope (Japan).

2.6.4. Immunohistochemistry

Immunohistochemical staining was performed using diaminobenzidine (SK-4103-100, Vector Laboratories, USA) to detect various markers of corneal epithelia, limbal, or conjunctival cells. The following primary antibodies were used: basal limbal epithelial markers—anti-p63α (1:100; 4892, Cell Signaling Technology Inc.) and anti-BMI-1 (1:100; sc-390443, Santa Cruz Biotechnology); stratum basale of the limbal epithelium—anti-CK-19 (1:200; PA5-95304, Invitrogen, USA); corneal epithelial markers—anti-stage-specific embryonic antigen-4 (SSEA4; 1:50; MAB1435, R&D Systems) and anti-CK-12 (1:250; MA5-42505, Invitrogen); conjunctival epithelium—CK-13 (1:200; sc-57003, Santa Cruz Biotechnology); and conjunctival epithelial mucus goblet cell markers—MUC-4 (1:500; MA5-42811, Invitrogen), and MUC-5 (1:500; WH0004586M7, Sigma-Aldrich).

2.7. Statistical analysis

The chi-square test (χ^2) was used to assess whether differences in scaffold integration were statistically significant.

For quantification of p63α expression following immunohistochemical staining, labeled cells were counted using ImageJ image-processing software. The percentage of p63α-positive cells was calculated in both limbal regions and in three randomly chosen corneal fields. Epithelial stratification was also considered by dividing the epithelium into layers and calculating marker distribution accordingly.

Normality of the data was assessed using the Shapiro–Wilk test. For normally distributed data, Student's *t*-test for independent samples was used (assuming equal variances. If variances were unequal, Welch's correction was applied. For non-normally distributed data, the Mann–Whitney *U* test was used. All statistical analyses were performed using GraphPad Prism 8.0 (Dotmatics, USA). A p-value < 0.05 was considered statistically significant.

3. Results

3.1. Macroscopic characterization and scaffold transparency

The 3D prints exhibited a perfect cylindrical shape and a 6 mm diameter as planned (Figure 1). Their thickness, measured by optical coherence tomography, was 110.6 ± 20.7 µm, comparable to that of the AM, which measured 113.2 ± 20 µm (Figure 1A). Each printed layer contributed approximately 50 µm of thickness, enabling reproducible and customizable scaffold thickness by adjusting the number of printed layers. Regarding transparency measurements, macroscopic images showed that the 3D-printed collagen scaffolds exhibited better transparency than AM in both light transmission and refraction, as assessed on a black background and a back-lit chart composed of parallel black lines (Figure 1B).

3.2. Differentiation kinetics of limbal stem cells on soft substrates

The results of hADSC differentiation into LSCs on 3D-printed collagen are shown in Figure 2. The results for plastic and AM substrates were previously published by Cadenas-Martín *et al.*[18] hADSCs seeded on the different substrates (plastic, AM, and 3D-printed collagen) significantly increased in average length during the first differentiation step toward ectoderm. However, in the second step, cells on all substrates significantly decreased in length, adopting the rounded morphology characteristic of LSCs (Figure 2A and C). Differences were also observed in cell numbers: on plastic and 3D-printed collagen, the cell count decreased during the second step (Figure 2B), whereas it increased on AM.

To compare the different substrates, the data were grouped into bar graphs. As shown in Figure 3A, cells seeded on culture plastic before differentiation were significantly more elongated than those on 3D-printed collagen and AM. However, although hADSCs seeded on 3D-printed collagen and AM reached similar lengths to those on plastic during the first differentiation step, they became significantly rounder by the end of the process. Specifically, cell length reduced to 50 µm on plastic, while it decreased to around 30 µm on 3D-printed collagen and AM (Figure 3A).

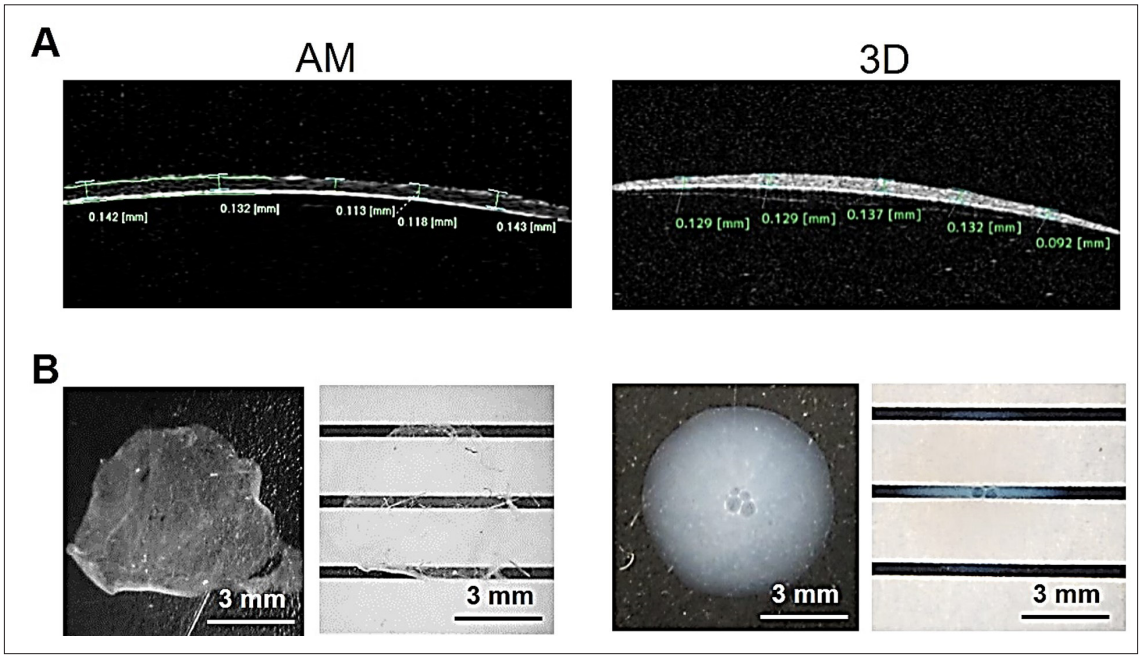

Figure 1. Macroscopic comparison between amniotic membrane (AM) and three-dimensional (3D) printed collagen scaffold. (A) Optical coherence tomography images showing thickness measurements in μm (in green). (B) Photographs illustrating light transmittance and refraction on a black and back-lit graphic background. Scale bar = 3 mm; magnification = 2×.

Figure 3B shows that hADSCs seeded on culture plastic proliferated significantly more than those on AM during the first step, although similar cell numbers were observed across all substrates after complete differentiation.

In summary, targeted differentiation into LSCs led to cell elongation during the first step and rounding during the second step on all substrates, with the shortening being more pronounced on 3D-printed collagen and AM than on plastic. Moreover, derivation of LSCs from hADSCs on 3D-printed collagen and AM showed faster kinetics, as cells acquired the rounded phenotype characteristic of LSCs within just 9 days of the second differentiation step.

3.3. Expression of limbal stem cell markers in human adipose-derived mesenchymal stem cell–derived cells on three-dimensional printed collagen

To assess the differentiation of hADSCs, the expression of LSC-specific markers was evaluated by immunofluorescence. After 10 days in the second differentiation step on 3D-printed collagen coated with vitronectin, 59% of the cells were double-positive for p63α and BMI-1 (Figure 4). When the culture period was extended to 11 days, the percentage of double-positive cells decreased slightly to 52% (Figure 4). Notably, at 13 days, this percentage dropped drastically to only 4% (Figure 4), suggesting that the LSCs actively differentiated toward corneal epithelial cells over time.

In agreement with these findings, 90.7% of cells on 3D-printed collagen were positive for the corneal epithelial marker SSEA-4 after 10 days in the second differentiation step (Figure 5). After 11 days, SSEA-4 positivity decreased to 36.8% (Figure 5), reinforcing the conclusion that 10 days of the second differentiation step represents the optimal time point for transplantation.

3.4. Re-epithelization outcomes in *in vivo* macroscopic study

Twelve rats were included and analyzed in the *in vivo* study: n = 3 for the cell-free AM group; n = 5 for the AM with ADSC-derived LSC group; and n = 4 for the 3D-printed collagen with ADSC-derived LSC group. Surface reepithelialization was evaluated using fluorescein staining after 10 days. In the cell-free AM group, one rat showed complete re-epithelization (absence of fluorescein; Figure 6A) while the remaining two showed nearly complete coverage (Figure 6B and C). In the AM + LSC group, three eyes were completely re-epithelialized (Figure 6D, F, and H), and two showed partial healing (Figure 6E and G). In the 3D-printed collagen + LSC group, three eyes were fully re-epithelized (Figure 6J, K, and L), and one remained partially re-epithelized (Figure 6I).

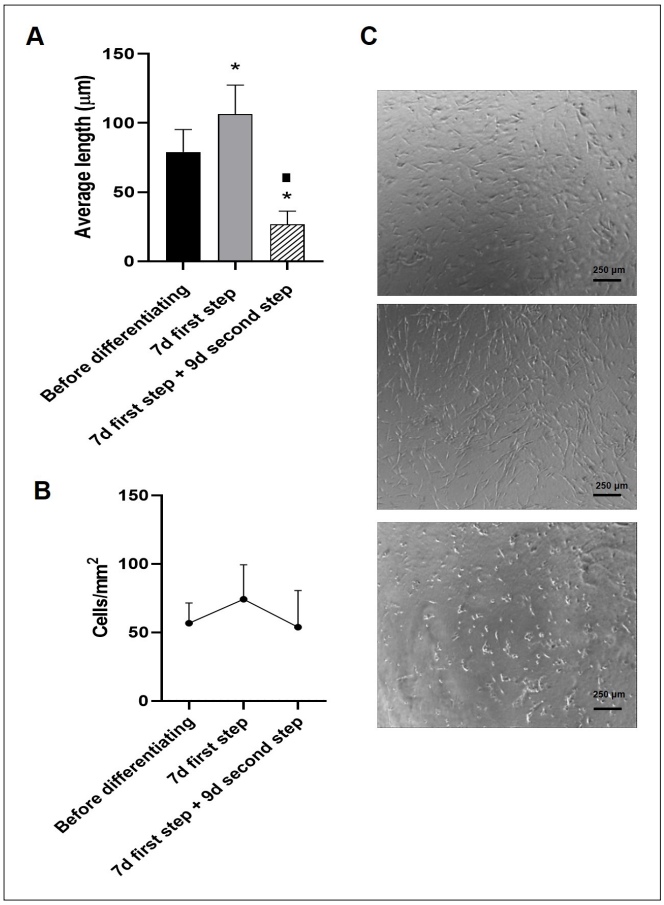

Figure 2. Differentiation kinetics, morphology, and cell numbers during differentiation of adipose-derived stem cells into limbal stem cells on three-dimensional printed collagen. (A) Average cell length (μm), (B) cell number per mm^2, and (C) phase contrast images before differentiation (top), after the first step (middle), and after the second step (bottom). Notes: Error bars indicate standard deviation. * indicates a statistically significant difference compared to human adipose-derived mesenchymal stem cells (hADSCs) before differentiation. ▪ indicates a statistically significant difference compared to hADSCs in the first differentiation step (* and ▪ = $p \leq 0.05$). Scale bar = 250 μm; magnification = 40×.

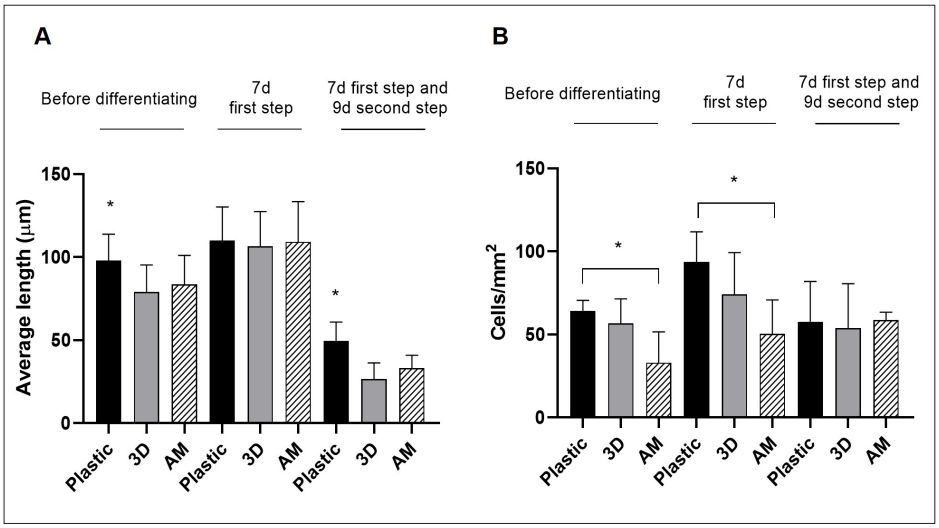

Figure 3. Comparison of morphometric analysis on the different substrates before and after each differentiation step. (A) Average cell length on plastic, three-dimensional printed collagen (3D), and amniotic membrane (AM). (B) Number of cells/mm^2 on plastic, 3D, and AM. Note: *$p \leq 0.05$.

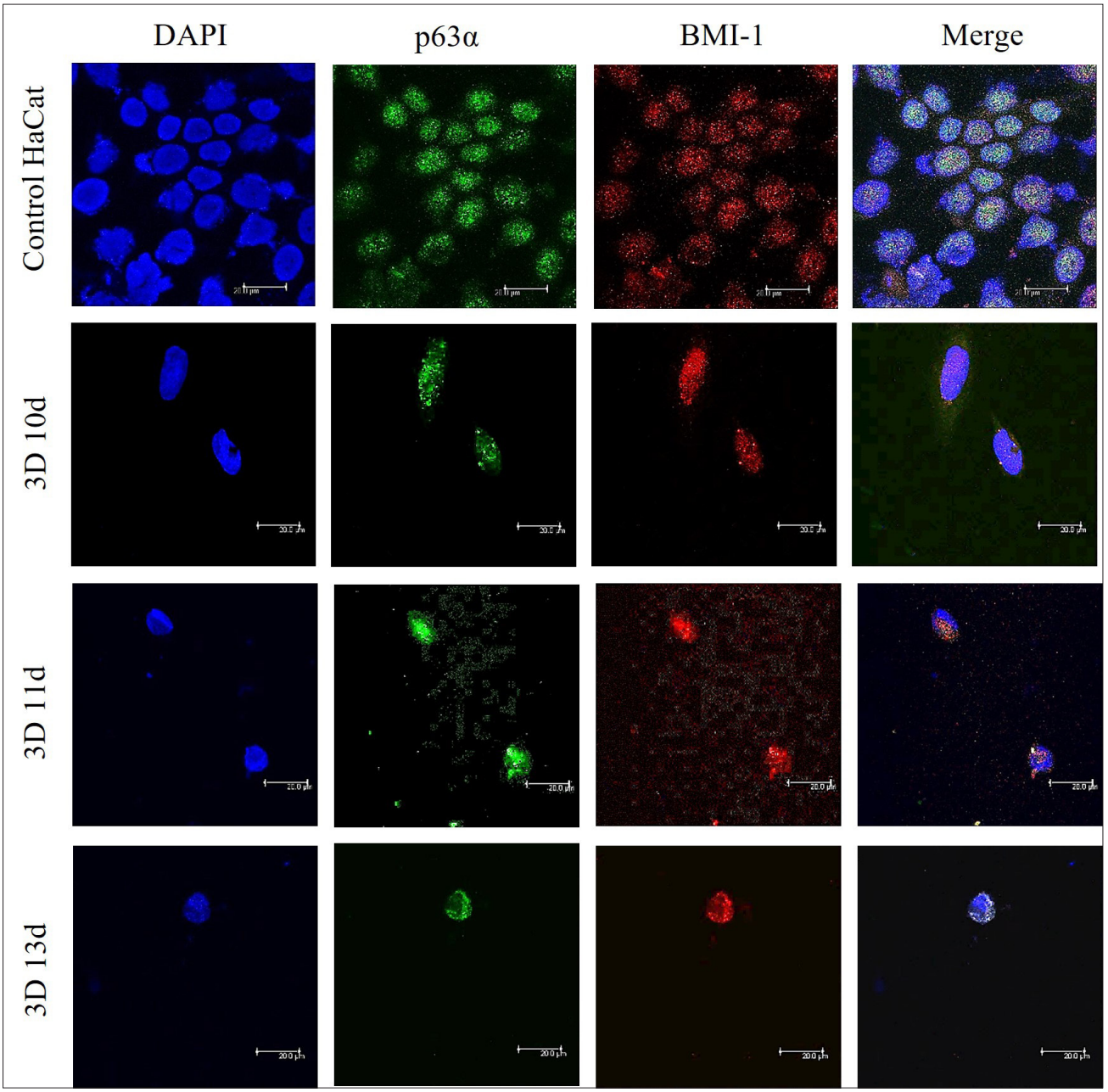

Figure 4. Confocal microscopy images showing double immunofluorescence for p63α/BMI-1 in human adipose-derived mesenchymal stem cell-derived limbal stem cells on three-dimensional printed collagen at different time points during the second differentiation step (10, 11, or 13 days). p63α appears in green, BMI-1 in red, and nuclei in blue (4',6-diamidino-2-phenylindole [DAPI]). HaCat cells grown to confluency were used as the positive control. Scale bar = 20 μm; magnification = 630×.

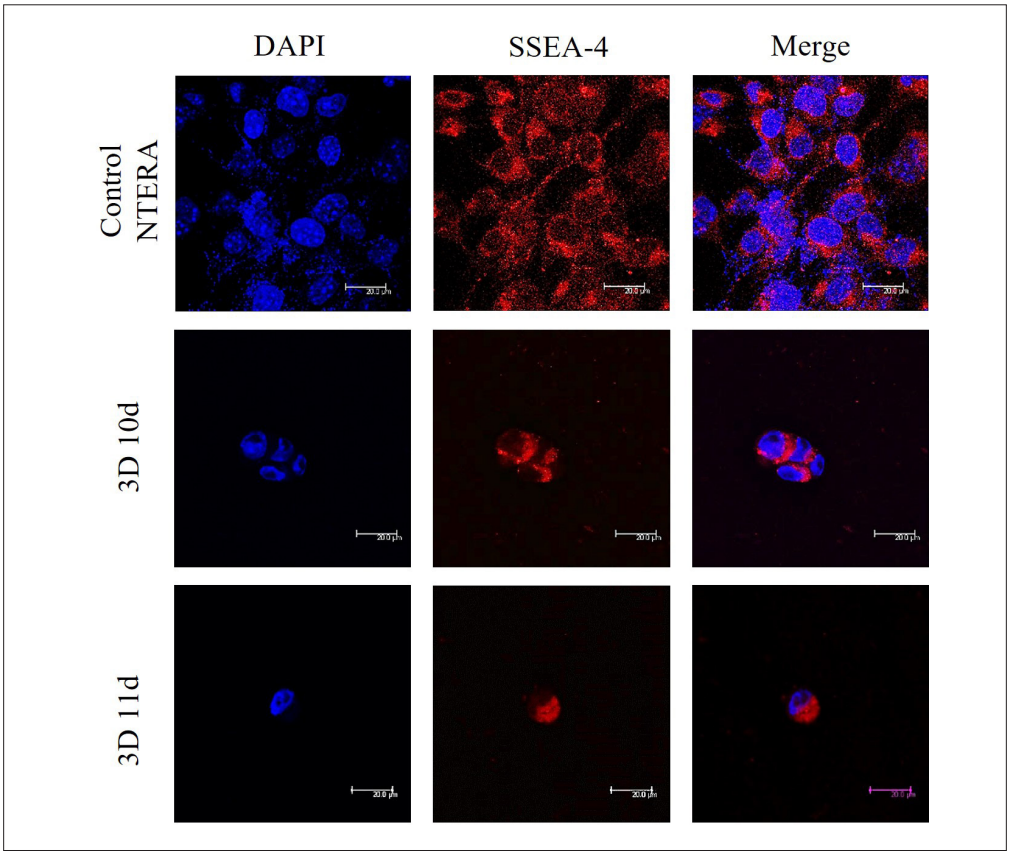

Figure 5. Confocal microscopy images of anti-stage-specific embryonic antigen-4 (SSEA4) immunofluorescence in three-dimensional (3D)-printed scaffolds with human adipose-derived mesenchymal stem cell-derived limbal stem cells after 10 or 11 days of the second differentiation step. SSEA4 is shown in red, and nuclei in blue (4',6-diamidino-2-phenylindole [DAPI]). NTERA cells grown to confluence served as the positive control. Scale bar = 20 μm; magnification = 630×.

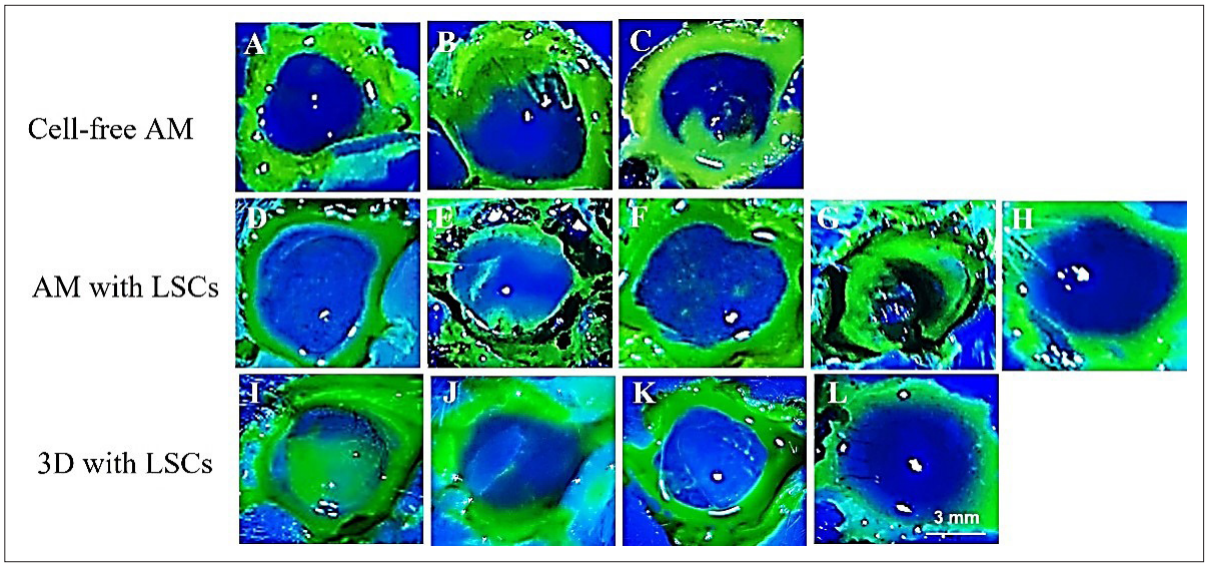

Figure 6. Macroscopic fluorescein staining images of rat eyes after amniotic membrane (AM) or three-dimensional (3D)-printed collagen transplantation. Areas of re-epithelization appear as an absence of fluorescein staining (blue), whereas persistent defects retain fluorescein (green). Scale bar = 3 mm; magnification = 10×. Abbreviation: LSC, limbal stem cells.

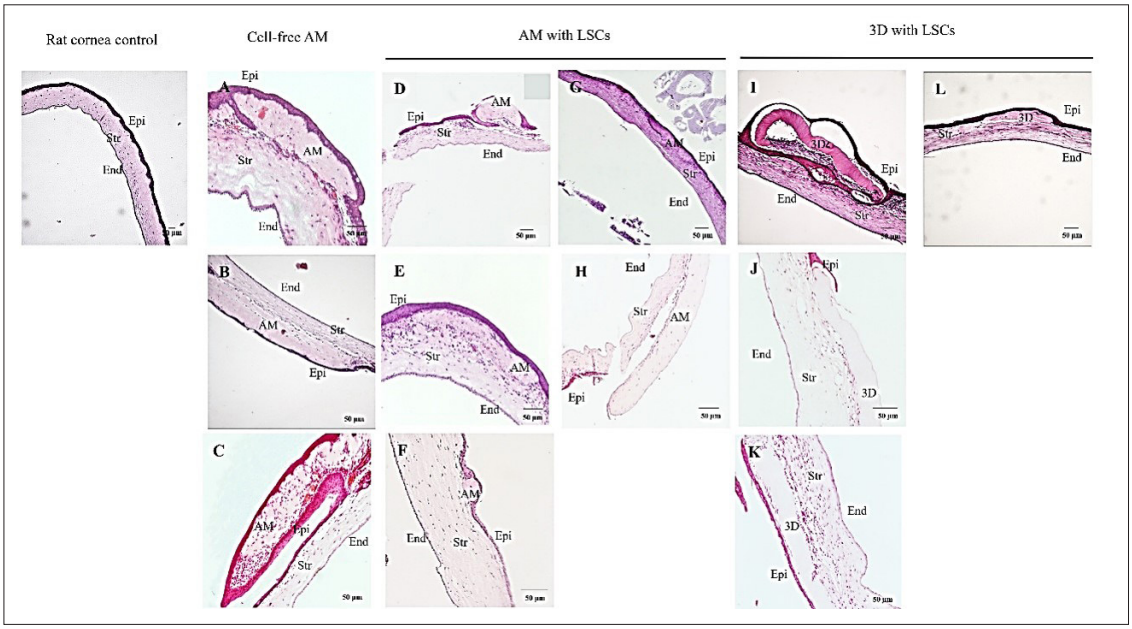

Figure 7. Hematoxylin-eosin-stained images of rat corneas after epithelial damage and scaffold transplantation. (A–C) Cell-free AM, (D–H) AM with LSCs, and (I–L) 3D with LSCs. Scale bar = 50 μm; magnification = (Control, G, L) 50×; (B–D, F, H–K) 100×, (A and E) 200×. Abbreviations: AM, amniotic membrane; End, corneal endothelium; Epi, corneal epithelium; LSCs, limbal stem cells; Str, corneal stroma; 3D, 3D-printed collagen.

In most cases, re-epithelization was nearly complete by day 10. A longer observation period would likely have resulted in full epithelial closure in all experimental groups.

3.5. Biocompatibility and superior integration of three-dimensional printed collagen scaffolds compared to amniotic membrane

Hematoxylin-eosin staining was performed on paraffin-embedded tissue sections to visualize the 3D-printed collagen and AM scaffolds (Figure 7). In the cell-free AM group, the scaffold was observed in all cases, but integration was evident in only one (Figure 7B). In the remaining rats, the cell-free AM was surrounded by epithelium, resulting in a regenerated epithelial layer and either partial or complete scaffold extrusion (Figure 7A and C).

In the AM with the LSC group, the AM was not integrated in two rats (Figure 7H) or was nearly completely surrounded by epithelium beneath it, suggesting impending extrusion (Figure 7D). However, in the remaining three rats, AM-LSC scaffolds were integrated with epithelial growth over the scaffold (Figure 7E, F, and G).

In the 3D-printed collagen with the LSC group, scaffolds were integrated in three out of four cases (Figure 7J, 7K, and 7L). In the remaining case, the scaffold was not integrated, and epithelial growth was observed surrounding it (Figure 7I).

With respect to scaffold biocompatibility, epithelial closure of the induced wound occurred in all groups, whether over or under the scaffold. The 3D-printed collagen with the ADSC-LSC group showed the highest integration rate (75%), followed by AM with ADSC-LSCs (60%) and cell-free AM (33%). A statistically significant difference was observed between the 3D-printed collagen with cells and the cell-free AM groups, suggesting that both the 3D-printed scaffold and the hADSC-derived LSCs actively contribute to scaffold integration (Table 1).

Table 1. Integration and epithelial growth rates (% of cases) after transplantation

Group	Number of rats	Rats with integrated scaffold (*n*)	Integration rate (%)	Epithelial growth (% of cases, underneath if not integrated)
Cell-free AM	3	1	33	100
AM with LSCs	5	3	60	100
3D with LSCs	4	3	75*	100

Note: * indicates statistical significance compared to cell-free AM at $p \leq 0.05$.

Abbreviations: AM, amniotic membrane; LSCs, limbal stem cells; 3D, 3D-printed collagen

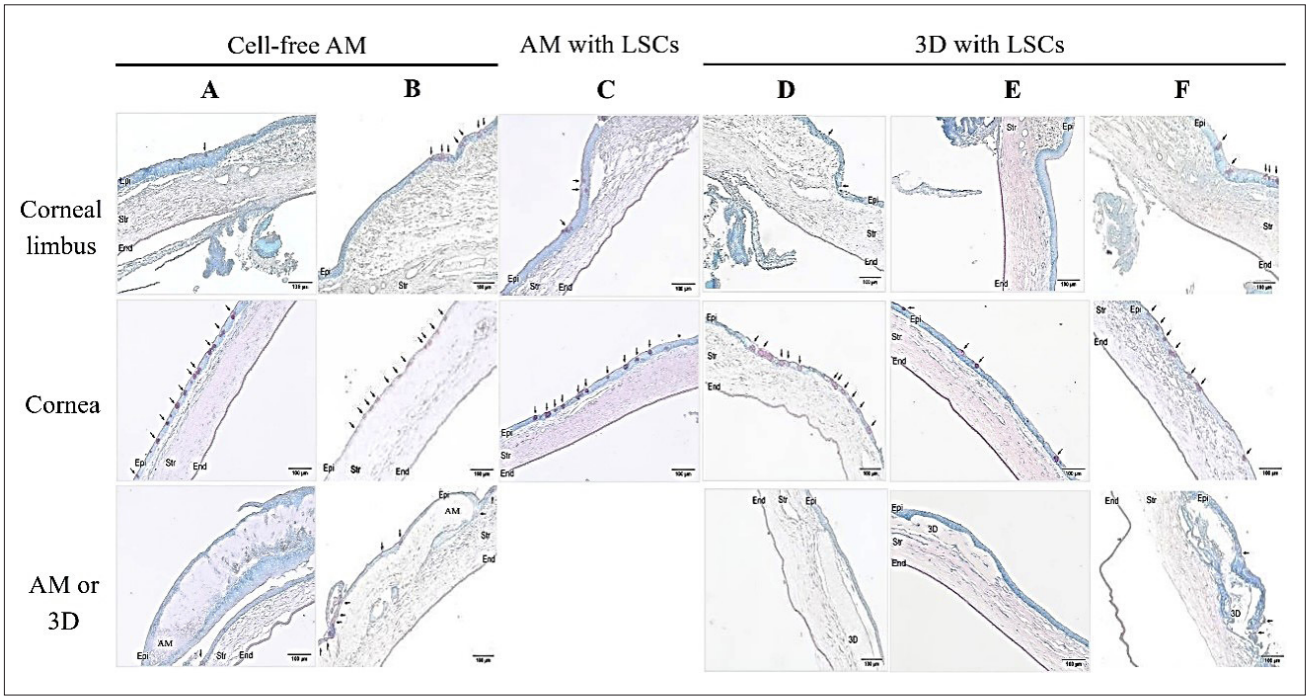

Figure 8. Periodic acid–Schiff staining of the corneal limbus, cornea, and scaffolds (AM or 3D), if present, in rats treated with (A–B) cell-free AM, (C) AM with ADSC-LSCs, and (D–F) 3D-printed collagen with ADSC-LSCs. Mucus goblet cells are stained pink (arrows). Scale bar = 100 μm; magnification = 100×. Abbreviations: ADSC-LSCs, adipose-derived mesenchymal stem cell–derived limbal stem cells; AM, Amniotic membrane; End, endothelium; Epi, epithelium; LSCs, limbal stem cells; Str, stroma; 3D, 3D-printed collagen.

3.6. Mucus conjunctival cells in the corneal epithelium revealed by periodic acid–Schiff staining

Periodic acid-Schiff staining demonstrated the presence of conjunctival mucus goblet cells in the corneal epithelium of all treatment groups, with variations depending on the treatment received. In the rats treated with cell-free AM, mucus cells were observed in both the sclerocorneal limbus and the corneal epithelium. Several PAS-positive cells were visible in the limbus and in the regenerated epithelium beneath the detached AM (Figure 8A and B). In one case, an increased number of mucus cells in the corneal epithelium near the limbus, although the central corneal region was absent and could not be assessed (not shown).

In the AM with the ADSC-LSC group, PAS-positive mucus cells were observed in the limbal regions of two animals, with additional labeled cells detected near one limbal area. Abundant MUC-positive cells in the corneal epithelium were identified in only one rat (Figure 8C). The AM scaffold was not present in any of the PAS-stained sections from this treatment group.

Rats treated with 3D-printed collagen with ADSC-LSCs showed PAS-positive cells in the corneal epithelium, while the limbus was largely negative. In one case, the epithelium preserved over the printed collagen scaffold lacked labeled mucus cells, although positive cells were observed in both limbal regions and the corneal epithelium (Figure 8D). In another case, mucus cells were found only in the corneal epithelium (Figure 8E). In the final case, both limbal regions and the corneal epithelium contained goblet cells, with some positive cells also present in the epithelium overlying the 3D-printed scaffold (Figure 8F).

3.7. Immunochemical evidence of regenerated conjunctival epithelium across all groups

3.7.1. Distribution of p63α-positive cells in limbal and corneal epithelia of control and treated corneas

Immunodetection of the p63α marker was positive (p63+) in all cases, with labeled cell nuclei in the limbal basal layer of both healthy rat corneas and all treated eyes. Interestingly, in both the undamaged negative control and all damaged and treated rats, $p63^+$ cells were detected not only in the basal layer of the limbal epithelium, as expected, but also throughout the basal layer of the corneal epithelium. In the human corneas used as positive controls, p63α was also detected in the basal layer of the corneal epithelium, although it was not detected in the limbal regions due to tissue loss after antigenic unmasking. Notably, all three treatments showed a higher number of $p63^+$ cells compared to the undamaged control rat, especially in the limbal region, which appeared considerably thinner in the control compared to the damaged and treated corneas. This suggests active limbal regeneration (Figure 9).

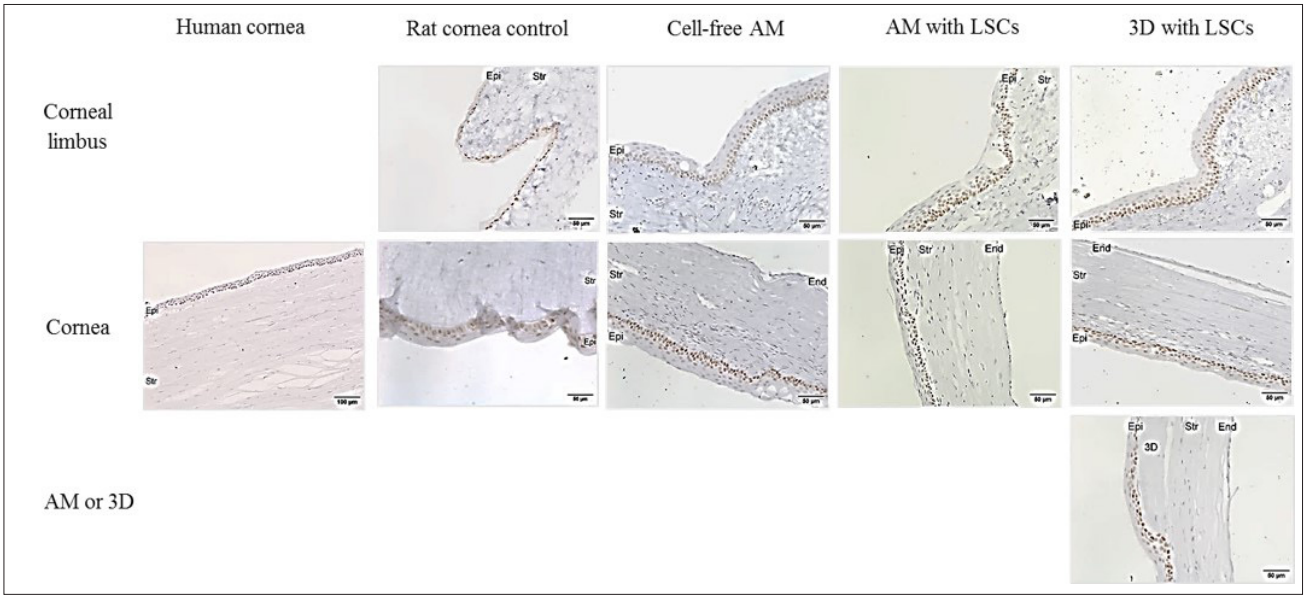

Figure 9. Positive labeling for p63α in the limbal and corneal epithelia of control and treated corneas. Positive cell nuclei appear brown. Scale bars = 100 μm (human cornea), 50 μm (rat corneas); magnifications = 100× (human cornea); 200× the rest, endothelium; Epi, epithelium; LSCs, limbal stem cells; Str, stroma; 3D, 3D-printed collagen scaffold.

To quantify the differences in the proportion of p63⁺-labeled cells between the control rat cornea and the various treatment groups, a general cell count was performed to calculate the percentage of positive cells in both limbal and corneal regions (Figures 10 and 11). No statistically significant differences were observed between the treatments and the healthy control, although individual variability was noted among rats within the same treatment group (data not shown). In the limbal epithelium, the proportion of p63α⁺ cells was 74% in the control, 64% in the cell-free AM, 66% in the AM with ADSC-LSC group, and 76% in the 3D-printed collagen with ADSC-LSC group (Figure 10A). However, differences in p63α labeling across epithelial layers may have masked overall results. Therefore, the distribution of p63⁺ cells across the different epithelial layers was also quantified, revealing significant differences between the control and the treatment groups. In the basal layer of the limbal epithelium, p63⁺ cells accounted for 93% in control samples, 92% in the cell-free AM group, 87% in the AM with ADSC-LSC group, and 95% in the 3D-printed collagen with ADSC-LSC group, though these differences were not statistically significant (Figure 10A). In the first suprabasal layer, statistically significant increases in p63⁺ cells were observed in all treatment groups compared to the control: 37% in the control, 79% in the cell-free AM group, 81% in the AM with LSC group, and 89% in the 3D-printed collagen with LSC group. In the second layer, p63α⁺ cells were absent in the healthy control but remained detectable in the treated groups, with significant differences: 66% in the cell-free AM group, 75% in the AM with ADSC-LSC group, and 70% in the 3D-printed collagen with ADSC-LSC group. In the third layer, similar results were observed but at lower proportions: 28% in the cell-free AM group, 38% in the AM with LSC group, and 44% in the 3D-printed collagen group, all significantly different from the control, which showed no p63α⁺ cells in that layer. These findings suggest that epithelial damage followed by any of the treatments promotes the expansion of p63α+ cells into the more superficial layers of the corneal epithelium. From the fourth layer onward, p63α⁺ cells were absent in all groups (Figure 10B).

In the corneal epithelium, statistically significant differences were observed between the healthy control and the damaged, treated groups. The control cornea exhibited 92% p63⁺ cells, compared to 63% in the cell-free AM group, 64% in the AM with LSC group, and 68% in the 3D-printed collagen with LSC group (Figure 11A). A statistically significant difference was noted between the cell-free AM group and 3D-printed collagen with LSCs, but not between the AM with and without cells, suggesting that the increased p63α presence may be attributed to the biomaterial rather than the cells. Layer-wise analysis in the corneal epithelium revealed no significant differences in the basal layer. In the first suprabasal layer, the percentages were 98% in the control, 64% in the cell-free AM group, 79% in the AM with LSC group, and 78% in the 3D-printed collagen with LSC group. Significant differences were observed between the control and the AM without cells. In the second layer, p63⁺ cell proportions dropped more sharply in the cell-free AM group (16%) compared to

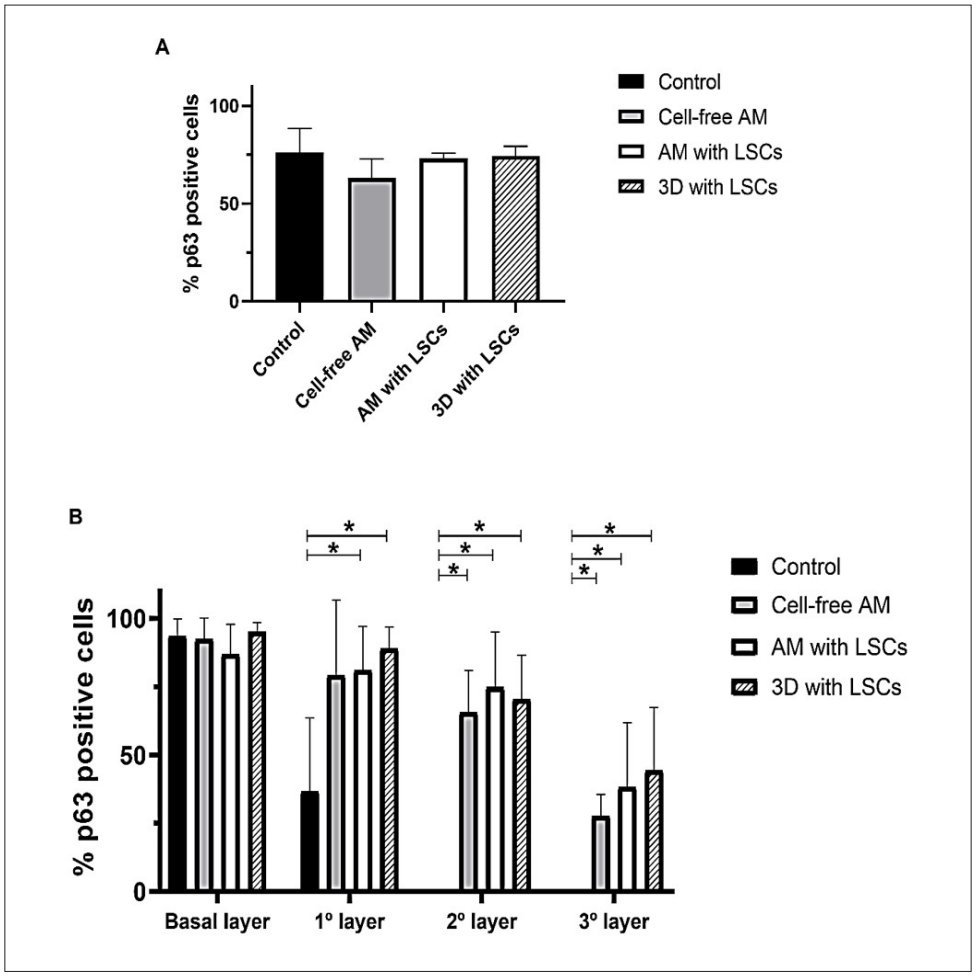

Figure 10. p63+ cell counts in the limbal epithelium. (A) Values across the entire epithelium, showing no significant differences between controls and treatments. (B) Proportion of p63+ cells per epithelial layer. Statistically significant differences (*) at $p \leq 0.05$ are observed between treatments within the same layer. Abbreviations: AM, amniotic membrane; LSCs, limbal stem cells; 3D, 3D-printed collagen scaffold.

the control (88%), AM with LSCs (54%), and 3D-printed collagen with LSCs (58%). In the third layer, an overall reduction was noted: 9% in the control, 6% in the cell-free AM group, 7% in the AM with LSC group, and 23% in the 3D-printed collagen with LSC group. Significant differences were found between the 3D-printed collagen group and both AM groups, regardless of cell inclusion (Figure 11B).

3.7.2. Limbal cell marker BMI-1-positive cells on the three-dimensional scaffold

The positive control tissues—human prostate and healthy rat cornea—showed limbal cell marker BMI-1$^+$ cells, located in the epithelium of the prostatic c-glands and in the stratum basale of the limbal and corneal epithelia, respectively (Figure 12A and B). In contrast, no positivity was generally detected in the treated eyes. BMI-1 labeling was observed in only one rat from the 3D-printed collagen with hADSC-derived LSC group, where several BMI-1$^+$ cells were found around the printed scaffold (Figure 12C). This suggests that these labeled cells may correspond to the transplanted human cells in this particular section.

3.7.3. Absence of cytokeratin 12 in the regenerated epithelium

Detection of CK-12 in the positive controls (human cornea and untreated healthy rat cornea) confirmed its established role as a specific marker of corneal epithelium. CK-12 strongly labeled the entire surface of the healthy corneal epithelium and clearly marked the transition zone at the sclerocorneal limbus, where conjunctival epithelium (negative for CK-12) begins. In contrast, no CK-12 labeling was observed in any of the rats subjected to epithelial damage and subsequent treatment. This result confirms that the regenerated epithelium was not of corneal origin and that the ADSC-LSCs did not differentiate into corneal epithelium (Figure 13).

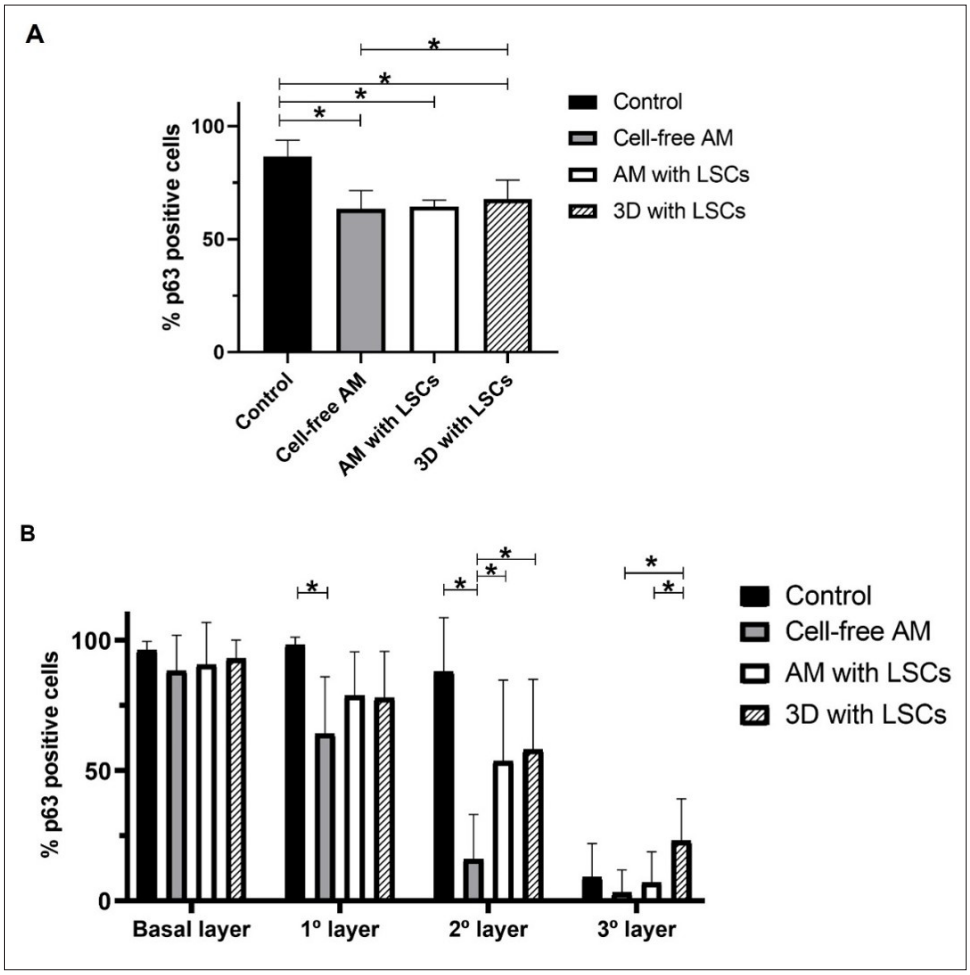

Figure 11. p63⁺ cell counts in the corneal epithelium. (A) Quantification of p63⁺ in the corneal epithelium. Significant differences (*) at $p \leq 0.05$ were observed between the healthy control and all treated groups, as well as between 3D-printed collagen with cells and cell-free AM. (B) Proportion of p63α⁺ cells per corneal epithelial layer. Statistically significant differences (*) at $p \leq 0.05$ are shown between treatments within the same layer. Abbreviations: AM, amniotic membrane; LSCs, limbal stem cells; 3D, 3D-printed collagen scaffold.

3.7.4. Non-specific cytokeratin 13 labeling in corneal and conjunctival epithelium

Although CK-13 is generally considered a marker for conjunctival epithelium, both the control human cornea and healthy rat cornea showed CK-13⁺ cytoplasmic labeling in the corneal and limbal epithelia as well. In the healthy rat cornea, labeled conjunctival epithelium was also distinguishable (Figure 14). In treated samples, CK-13 labeling was observed in the conjunctival, limbal, and corneal epithelia of all rats, with no clear differences between treatment groups. Positive labeling was also detected in epithelial layers located above and below both the AM and 3D-printed collagen scaffolds when present (Figure 14). Hence, CK-13 did not provide further insight into the nature of the regenerated epithelium.

Other epithelial markers, including SSEA-4 (corneal), MUC-4 and MUC-5 (conjunctival), and CK-19 (limbal), were not conclusive in determining cell identity (results not shown).

4. Discussion

In this study, hADSCs were differentiated into LSCs within a 3D-printed collagen I scaffold for transplantation into a rat model of total LSCD. The aim was to evaluate its biocompatibility and regenerative capacity in comparison with standard AM transplantation. We achieved successful *in vitro* differentiation of hADSCs into LSCs, as confirmed by the expression of specific markers, and observed superior *in vivo* scaffold integration compared to AM. However, analysis of structural markers revealed that the regenerated epithelium was conjunctival rather than corneal, indicating that the contribution of ADSC-LSCs was insufficient for complete corneal re-epithelization. *In vitro*, it was observed that during ectodermal induction, the cells initially elongated and then, with SHEM

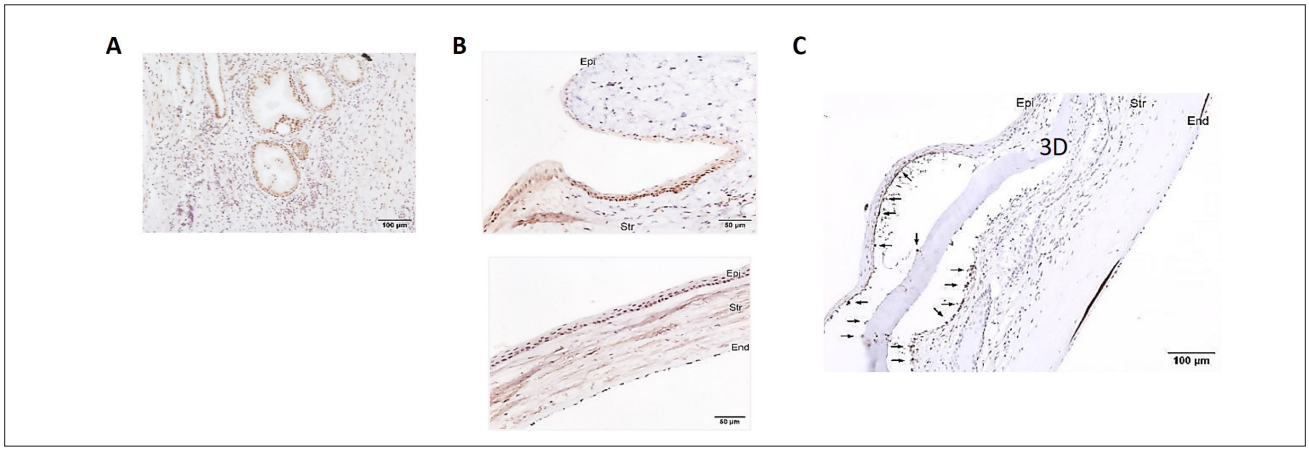

Figure 12. Results of anti-BMI-1 immunohistochemistry. Positive brown nuclear labeling is seen (A) in the epithelium of human prostate glands, and (B) in the stratum basale of the limbal and corneal epithelium of a healthy rat cornea. (C) Detail of the three-dimensional (3D)-printed collagen scaffold with ADSC-LSCs, showing BMI-1$^+$ cells around the scaffold (arrows). An empty space artifact is visible, caused by differential dehydration of the printed collagen relative to the corneal stroma during processing. Scale bars = 50 µm (B), 100 µm (A, C); Magnifications = 200× (B),100× (A, C). Abbreviations: ADSC-LSCs, adipose-derived mesenchymal stem cell–derived limbal stem cells; End, endothelium; Epi, epithelium; Str, stroma.

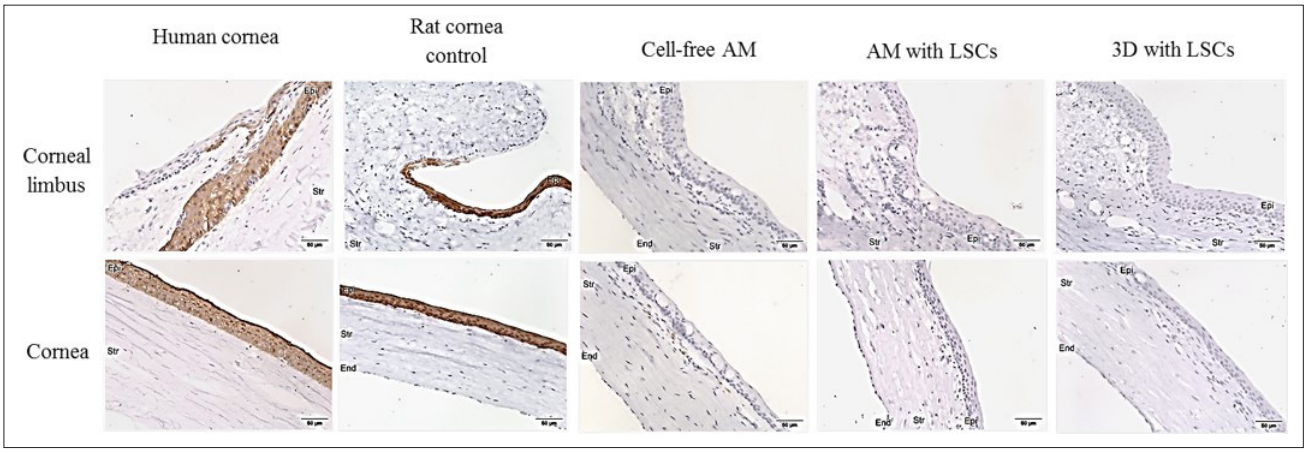

Figure 13. Results of anti-cytokeratin 12 immunohistochemistry. Positive brown cytoplasmic labeling is present only in corneal epithelial cells. Scale bar = 50 µm; Magnification = 200×. Abbreviations: AM, amniotic membrane; End, endothelium; Epi, epithelium; LSCs, limbal stem cells; Str, Stroma; 3D, 3D-printed collagen.

medium supplemented with PEDF and KGF, they became statistically significantly more rounded, similarly to those on AM.[18] Directed differentiation on 3D-printed collagen and AM soft scaffolds showed faster kinetics than on plastic. Only nine days of culture were required in the second differentiation step to acquire the rounded morphology with a high nucleus-to-cytoplasm ratio characteristic of LSCs, compared to the 13 days needed on plastic culture surfaces.

When comparing the average cell length, hADSCs seeded on 3D-printed collagen and AM were significantly shorter both before differentiation and after differentiation than those seeded on culture plastic. This may be due to the fact that soft substrates lead to decreased maturation of focal adhesions, lower stress fiber content, and reduced nuclear stretch—conditions that promote the development of LSCs. Indeed, MSCs cultured on soft substrates have been shown to acquire a relaxed state caused by low cell contractility and stiffness, which correlates with increased reprogramming efficiency and, therefore, earlier colony formation compared to cells seeded on stiff substrates.[33] This explains the improved differentiation efficiency observed on 3D-printed collagen and AM.

Regarding cell count, hADSCs actively replicated during ectodermal induction on all substrates. Subsequently, in the case of 3D-printed collagen and plastic, cell numbers decreased to their initial levels.[18] This initial increase may have been due to the composition of the induction medium, which contains a higher proportion of FBS (15%) than the SHEM medium (2%).[31] The subsequent decrease in cell number

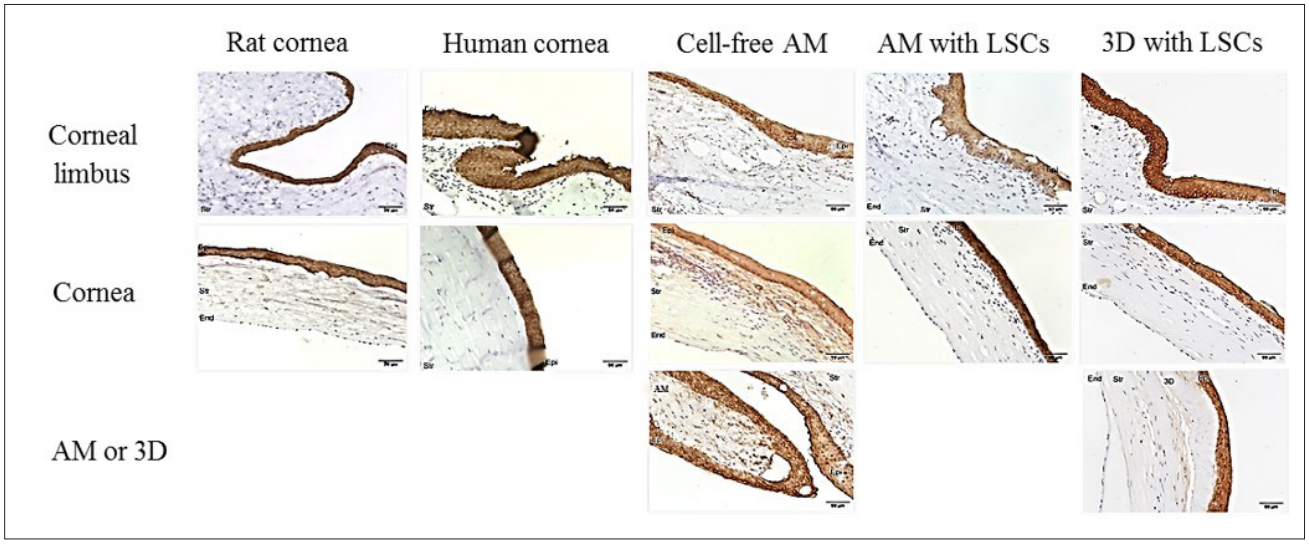

Figure 14. Results of anti-cytokeratin 13 immunohistochemistry. Positive brown cytoplasmic labeling is present in both corneal and limbal epithelial cells. Scale bar = 50 μm; magnification = 200×. Abbreviations: AM, amniotic membrane; End, endothelium; Epi, epithelium; LSCs, limbal stem cells; Str, stroma; 3D, 3D-printed collagen.

during the second stage of differentiation could be attributed to the differentiation process itself and the acquisition of a slower cell cycle, which is a known characteristic of stem cells.[1]

The only widely accepted marker of limbal cells is p63α,[14] but it is not present in all limbal niche cells. Therefore, we also evaluated the expression of potential differentiation markers such as BMI-1 and SSEA-4, given the lack of a consensus panel of markers for LSCs. LSCs have been shown to co-express BMI-1 and p63α under conditions of normal homeostasis, identifying human limbal holoclones.[10] In contrast, SSEA-4 has been described as a marker for stem cells but also for differentiated corneal epithelial cells.[9] One study reports 12% of hADSCs as positive for SSEA-4,[34] while another claims no expression.[35] Compared to the results on AM and plastic published in Cadenas-Martín *et al.*[18], hADSC-derived LSCs cultured for 10 days in SHEM medium supplemented with PEDF and KGF (second differentiation stage) showed 53.3% double-positive cells for p63α/BMI-1 on plastic, increasing to 59% on 3D-printed collagen. When culture for one additional day, the percentage of double-positive cells decreased to 43.4% on plastic and 52% on 3D-printed collagen. Interestingly, while this percentage remained relatively stable on plastic in extended cultures (41.4% at 13 days), it dropped drastically on 3D-printed collagen to only 4%, suggesting active differentiation of LSCs into corneal epithelial cells in the 3D scaffold. On AM, the percentage of p63α/BMI-1-positive cells at 13 days was 34.1%. These findings indicate that, despite reaching a similar number of cells across all substrates, differentiation efficiency and kinetics were higher on the 3D-printed collagen scaffold than on AM or culture plastic.

This is consistent with results obtained for the corneal epithelium marker SSEA-4, which showed 52.9% positivity on plastic,[18] compared to 90.7% on 3D-printed collagen at day 10 of the second differentiation step. As previously mentioned, this high percentage may reflect either a population of more differentiated corneal epithelial cells or residual undifferentiated hADSCs. Nonetheless, the presence of undifferentiated hADSCs within the LSC population could be beneficial, as they express epithelial markers such as ABCG2, p63α, CK12, and CK76, making them a suitable cell source for LSCD treatment.[36] These results suggest that 10 days of the second differentiation step represents the optimal time point for transplantation. Among the substrates tested, 3D-printed collagen proved to be the most efficient for differentiation, yielding the highest percentage of hADSC-derived LSCs expressing the specific markers used. Moreover, the use of ADSC-derived LSCs not only eliminates the need for a corneal donor but also avoids donor-dependent variation in the expression of epithelial and LSC markers.[37]

In vivo, biocompatibility and re-epithelization were achieved in all treatment groups, including AM with or without LSCs (controls) and 3D-printed collagen with LSCs. Hematoxylin staining confirmed 100% re-epithelization above and/or below the scaffolds, with wound closure observed in all cases. The 3D-printed collagen with the LSC group showed the highest statistically significant integration rate (75%), demonstrating superior biocompatibility and safety. Significant differences were observed between the 3D-printed collagen with cells and the cell-free AM groups,

suggesting that hADSC-derived LSCs actively contribute to scaffold integration.

To ascertain whether the nature of the epithelium was corneal or conjunctival, the following putative specific markers were studied: for the corneal limbus (p63α,[12] BMI-1,[10] CK-19,[11] and SSEA-4[9]); for the corneal epithelium (CK-12[7] and SSEA-4[9]); and for the conjunctival epithelium (MUC-4, MUC-5, and CK-13[13]). Surprisingly, in healthy eye controls, the presence of several of these markers did not match previously published data. Positive p63α labeling was observed in the stratum basale of both the limbal and corneal epithelium in healthy human and rat corneas, and in the stratum basale and several suprabasal layers of the limbal and corneal epithelium in all treated rats. However, Di Iorio *et al.*[38], using the 4A4 pan-p63 monoclonal antibody from BD Biosciences, which detects all p63 isoforms and allows differentiation between them by Western blot, found that the p63α isoform was restricted to the basal layer of the limbal epithelium in healthy corneas. In damaged corneas, their results aligned with ours, showing p63α expression extending throughout the corneal stratum basale and into several suprabasal layers of both the limbal and corneal epithelium. Collin *et al.*,[39] who used the same antibody as in our study (anti-p63α from Cell Signaling), reported identical findings to ours, with p63α expression observed throughout the basal epithelium of the corneal surface. The difference in p63α detection in the stratum basale of the healthy corneal epithelium between the two studies may be attributed to discrepancies in antibody specificity. The anti-p63α antibody used in our study detects two isoforms of p63α: the full-length TAp63α, which contains an amino-terminal transactivation domain, and the truncated ΔNp63α, which lacks this domain. In the human corneal epithelium, ΔNp63α is the predominant isoform and is crucial for the differentiation of TACs,[12] while TAp63α, which is highly expressed in the limbal epithelium, is involved in maintaining less differentiated limbal cells.[40] In addition, TAp63α is required for the initiation of epithelial stratification, while ΔNp63α is essential for maintaining epithelial differentiation.[41] According to Verma *et al.*,[42] the corneal epithelial cells generated by LSCs distribute across the corneal surface depending on their degree of maturation. When the cornea is damaged, limbal cells, positive for ΔNp63α, proliferate and migrate along the stratum basale of the corneal epithelium, maintaining ΔNp63α expression.[12] This could explain our findings, in which ΔNp63α is likely being detected in the stratum basale epithelium of control corneas, while both TAp63α and/or ΔNp63α are detected in damaged corneas.

Quantitatively, a greater number of suprabasal layers in both the limbal and corneal epithelia was observed in all treated rats compared to the healthy control corneas. Despite showing a higher proportion of p63α$^+$ cells in the corneal epithelium, the healthy corneas had a statistically lower number of epithelial layers, which may reflect the proliferation-inducing effect of the treatments. Among the treatments, the cell-free AM group showed the lowest proportion of p63α$^+$ cells in both the limbus and cornea, although this group exhibited high variability. This may be due to inconsistent membrane orientation during surgery; the epithelial side of the AM could not always be placed facing the damaged corneal surface, as recently emphasized by Bisevac *et al.*[20] Nevertheless, the AM treatments (with or without cells) showed no significant differences, except in the upper layers of the corneal epithelium in the AM-LSC-treated group, suggesting that the presence of LSCs enhances tissue regeneration, albeit modestly. Importantly, the statistically significant difference in the group treated with the 3D-printed collagen with cells indicates that the primary contributing factor is the biomaterial used as the scaffold.

Regarding BMI-1, although positive controls showed its presence in the basal layer of the peripheral corneal and limbal epithelium, in the treated corneas, BMI-1$^+$ cells were observed around the 3D print in only one rat, suggesting that the transplanted LSCs remained attached to the 3D scaffold. Previous studies indicate that in humans, BMI-1 is expressed during the embryonic period in corneal cells that are also p63$^+$, and that after birth, BMI-1 becomes restricted to the corneal limbus,[10] with expression being lost as LSCs proliferate and migrate to repair damage.[42] This differs in murine models, where BMI-1 expression appears to be age-dependent. BMI-1 expression has been detected in the basal and suprabasal layers from before epithelial stratification until eight weeks of age, after which only isolated colonies of small BMI-1$^+$ cells are observed, which eventually disappear.[43] This supports the interpretation that the BMI-1$^+$ cells detected around the 3D print were transplanted LSCs. On the other hand, the absence of positive BMI-1 labeling in the rest of the epithelium indicates that either most of the transplanted cells did not remain in place, were not present in the sections analyzed, or had differentiated *in situ*. Increasing the number of LSCs seeded on the scaffolds or enhancing their attachment may improve outcomes. Despite this, the presence of BMI-1$^+$ cells on the 3D print suggests that it is superior to AM in supporting the survival of transplanted human LSCs until the end of the *in vivo* study.

Immunodetection of cytokeratin 12 confirmed that the regenerated epithelium on the corneal surface in our study is not corneal epithelium. CK-12 is a recognized marker of corneal epithelium,[7] and was detected in the positive controls, clearly labeling the entire surface of the healthy corneal epithelium and allowing identification of the transition point between the corneal and conjunctival epithelia (negative for CK-12) in the sclerocorneal limbus. No CK-12 was detected in the damaged and treated corneas, suggesting that the regenerated epithelium is not corneal in nature.

Cytokeratin 13 is a recognized marker for conjunctival epithelium,[44] typically found in the suprabasal stratum of the limbal epithelium and in all layers of the conjunctiva, while being absent in the corneal epithelium.[45] However, in our study, both the control human and healthy rat corneas showed CK-13 labeling in the corneal and limbal epithelia. Treated rats also showed CK-13$^+$ labeling in all layers of the regenerated corneal epithelium; hence, this marker does not further clarify the nature of the regenerated tissue.

Consistent with these findings, PAS staining highlighted the presence of mucus-secreting cells typical of conjunctival epithelium in the regenerated corneal surface across all treatments, supporting the conclusion that the regenerated epithelium is conjunctival. Some variation in the number of mucus-secreting cells was observed between treatments with and without LSCs, with a greater number of labeled cells found in the acellular group. This may indicate the presence of a lower-quality epithelium with reduced transparency (although conjunctival in all cases) in the standard bare AM treatment, supporting the further development of cell therapies using cultured LSCs for corneal surface reconstruction.

Many researchers have studied the use of MSCs to address LSCD or corneal epithelial damage.[46] The ability of these cells to differentiate into LSCs makes them ideal, especially for the treatment of bilateral LSCD, where an autologous extraocular source is needed. ADSCs cultured with LSC-specific medium improved anti-inflammatory and anti-angiogenic paracrine profile, in addition to improving wound healing in the rat LSCD model through a paracrine mechanism,[16] as in this study. Overall, our study supports the favorable effect of hADSC-derived LSCs on corneal epithelial regeneration, with an improved reparative response observed in cell-based treatments. Both groups of rats treated with AM with cells and 3D-printed collagen with cells had a higher proportion of p63α progenitor cells (and in the case of 3D-printed collagen, also BMI-1), and a lower number of mucus cells, which would support enhanced corneal transparency. Furthermore, among the cell-based treatments, the 3D collagen I print appeared to generate a more favorable response, supporting the viability of transplanted LSCs during re-epithelization and promoting increased proliferation of p63$^+$ cells.

Regarding carriers, AM is the most commonly used carrier for ocular surface reconstruction,[47] as its composition—rich in type I and III collagens—mimics, to some extent, the extracellular matrix composition of the limbal niche. In addition, it possesses anti-inflammatory, antimicrobial, and anti-angiogenic properties. However, the success rate of reepithelialization seems to depend on the integrity of the membrane and the amount of growth factors it releases; thus, the results obtained vary depending on how the membrane is handled and on donor-specific characteristics. AM use also presents several drawbacks, such as batch-to-batch variability, limited availability, potential risk of infectious disease transmission, and low transparency.[48] In our case, we used type I collagen, as it is one of the most widely used biomaterials for tissue engineering applications due to its biocompatibility and low immunogenicity.[49] Moreover, it is the main component of the cornea and has long been considered a suitable substrate as an epithelial cell carrier,[24] potentially helping to address shortages of donor corneas and AM and offering a more affordable alternative treatment. In fact, *in vivo* studies have already demonstrated that bovine dermis-derived type I collagen implants, even without 3D printing, integrate and promote reepithelialization in anterior lamellar keratoplasty models in rabbits.[50] Simpson *et al.*[51] used an inflammation-suppressing phosphorylcholine coating on a collagen analogue peptide implant conjugated to polyethylene glycol, which enhanced the corneal regenerative response by accelerating nerve regeneration and corneal sensory recovery. This suggests further improvements may be possible by incorporating supplements into our collagen I print to enhance the quality of regeneration.

In a recent collaborative study, Edel *et al.*[19] used an *in vivo* LSCD model and generated induced pluripotent stem cells (iPSCs) from bone marrow mesenchymal stem cells, which were subsequently differentiated into LSCs (iPSC-LSCs). Differentiation was performed in two stages: the first lasted 4 days and used the same supplements as Cadenas-Martin *et al.*[18] but in E6 medium without FBS; the second stage lasted another 11 days and used commercial CnT30 epithelial differentiation medium to obtain LSCs. These cells were seeded on fibrin gel patches coated with laminin or collagen IV instead of vitronectin. The cells were positive for p63α, CK-3, and CK-12, and by day 30, they showed structural regeneration of the epithelium.[19]

5. Conclusion

Our results suggest that, similar to AM and fibrin, 3D-printed collagen may serve as an alternative carrier for corneal epithelial reconstruction. Furthermore, it offers advantages: collagen does not degrade as quickly as fibrin, integrates better than AM, and could mimic the 3D topography of the Palisades of Vogt, where LSCs are located,[52] thus improving biocompatibility. Moreover, its thickness can be customized to facilitate handling,[53] allowing for the development of a substitute with greater transparency, stability,[54] and adaptation to patient-specific requirements.

Acknowledgments

The authors would like to thank the La Paz Biobank and the Image and Immunohistochemistry and Cell Culture platforms for the use of their facilities and technical assistance. They also thank Francisco Navarro, Paula Linzoaín, and Elsa Umiri for their technical support. The authors further acknowledge Morote Traducciones for the English editing.

Funding

The authors received grants from: the Ministry of Science and Innovation, Strategic Health Action, Instituto de Salud Carlos III (ISCIII), Proyectos de I+D+I en Salud (grant number PI23/00207) and co-funded by the European Union; as well as the Foundation for Biomedical Research of La Paz University Hospital (Luis Álvarez Projects; grant number 07/252898.9/24). The study was also supported by StemVision and Carl Zeiss AG. M. Cadenas-Martín and M. Stokking were financed by the European Social Fund (PI_SEPE_MPDM PROGRAMA INVESTIGO 1785344099 and PI_SEPE_PROGRAMA INVESTIGO 26-23, respectively).

Conflict of interest

The authors declare that the research was conducted in the absence of any commercial or financial relationships that could be construed as a potential conflict of interest.

Author contribution

Conceptualization: Maria P. De Miguel

Formal analysis: Marta Cadenas-Martín, Martha Stokking, Ana I. Martín-González, Alba Fernández-Ferrer, Francisco Arnalich-Montiel, Maria P. De Miguel

Funding acquisition: Maria P. De Miguel, Francisco Arnalich-Montiel

Investigation: Marta Cadenas-Martín, Martha Stokking, Ana I. Martín-González, Alba Fernández-Ferrer, Francisco Arnalich-Montiel, Maria P. De Miguel

Methodology: Marta Cadenas-Martín, Martha Stokking, Ana I. Martín-González, Alba Fernández-Ferrer, Francisco Arnalich-Montiel, Maria P. De Miguel

Project administration: Maria P. De Miguel

Resources: Maria P. De Miguel, Francisco Arnalich-Montiel

Supervision: Maria P. De Miguel

Validation: Marta Cadenas-Martín, Martha Stokking, Ana I. Martín-González, Alba Fernández-Ferrer, Francisco Arnalich-Montiel, Maria P. De Miguel

Writing-original draft preparation: Marta Cadenas-Martín, Martha Stokking, Ana I. Martín-González, Alba Fernández-Ferrer, Francisco Arnalich-Montiel, Maria P. De Miguel

Writing-review and editing: Marta Cadenas-Martín, Martha Stokking, Ana I. Martín-González, Alba Fernández-Ferrer, Francisco Arnalich-Montiel, Maria P. De Miguel

Ethics approval and consent to participate

The study was conducted in accordance with the guidelines of the Declaration of Helsinki, and was approved by the Institutional Review Boards of La Paz Hospital (protocol code PI308, 2/4/2004) and Ramon y Cajal Hospital (protocol code 305/11, 10/1/2011). Informed consent was obtained from the tissue donors involved in the study.

Consent for publication

Informed consent for publication was obtained from all subjects involved in the study.

Availability of data

Data obtained from this study can be requested from the corresponding author upon reasonable request.

References

1. De Miguel MP, Casaroli-Marano RP, Nieto-Nicolau N, *et al*. Frontiers in regenerative medicine for cornea and ocular surface. In: *Frontiers in Stem Cell and Regenerative Medicine Research*. Vol 1. Bentham Science Publishers; 2015:92-138. doi: 10.2174/978160805994211501006

2. Zavala J, López Jaime GR, Rodríguez Barrientos CA, Valdez-Garcia J. Corneal endothelium: developmental strategies for regeneration. *Eye (Basingstoke)*. 2013;27(5):579-588. doi: 10.1038/eye.2013.15

3. Akanda ZZ, Naeem A, Russell E, Belrose J, Si FF, Hodge WG. Graft rejection rate and graft failure rate of penetrating keratoplasty (PKP) vs lamellar procedures: a systematic review. *PLoS One*. 2015;10(3):e0119934. doi: 10.1371/journal.pone.0119934

4. Popova P, Malalana F, Biddolph S, *et al*. Interspecies comparative morphological evaluation of the corneal epithelial stem cell niche: a pilot observational study. *J Vet Sci*. 2022;23(4):e62. doi: 10.4142/JVS.22009

5. Fernández A, Moreno J, Prósper F, García M, Echeveste J. *Regeneration of the ocular surface: stem cells and reconstructive techni-ques*. *An Sist Sunit Navar*. 2008; 31(1): 53-69. doi: 10.4321/s1137-66272008000100005

6. Nuzzi A, Pozzo Giuffrida F, Luccarelli S, Nucci P. Corneal epithelial regeneration: old and new perspectives. *Int J Mol Sci*. 2022;23(21):13114. doi: 10.3390/ijms232113114

7. Tanifuji-Terai N, Terai K, Hayashi Y, Chikama TI, Kao WWY. Expression of keratin 12 and maturation of corneal epithelium during development and postnatal growth. *Invest Ophthalmol Vis Sci*. 2006;47(2):545-551. doi: 10.1167/iovs.05-1182

8. Kayama M, Kurokawa MS, Ueno H, Suzuki N. Recent advances in corneal regeneration and possible application of embryonic stem cell-derived corneal epithelial cells. *Clin Ophthalmol*. 2007;1(4):373-382.

9. Truong TT, Huynh K, Nakatsu MN, Deng SX. SSEA4 Is a potential negative marker for the enrichment of human corneal epithelial stem/progenitor cells. *Invest Ophthalmol Vis Sci*. 2011;52(9):6315-6320. doi: 10.1167/iovs.11-7518

10. Barbaro V, Testa A, Di Iorio E, Mavilio F, Pellegrini G, De Luca M. C/EBPδ regulates cell cycle and self-renewal of human limbal stem cells. *J Cell Biol*. 2007;177(6):1037-1049. doi: 10.1083/jcb.200703003

11. Polisetti N, Sharaf L, Schlötzer-Schrehardt U, Schlunck G, Reinhard T. Efficient isolation and functional characterization of niche cells from human corneal limbus. *Int J Mol Sci*. 2022;23(5):2750. doi: 10.3390/ijms23052750

12. Novelli F, Ganini C, Melino G, *et al*. p63 in corneal and epidermal differentiation. *Biochem Biophys Res Commun*. 2022;610:15-22. doi: 10.1016/j.bbrc.2022.04.022

13. Ramos T, Scott D, Ahmad S. An update on ocular surface epithelial stem cells: cornea and conjunctiva. *Stem Cells Int*. 2015;2015:601731. doi: 10.1155/2015/601731

14. Pellegrini G, Rama P, Matuska S, *et al*. Biological parameters determining the clinical outcome of autologous cultures of limbal stem cells. *Regenerative Med*. 2013;8(5):553-567. doi: 10.2217/rme.13.43

15. Galindo S, Herreras JM, López-Paniagua M, *et al*. Therapeutic effect of human adipose tissue-derived mesenchymal stem cells in experimental corneal failure due to limbal stem cell niche damage. *Stem Cells*. 2017;35(10): 2160-2174. doi: 10.1002/stem.2672

16. Nieto-Nicolau N, Martínez-Conesa EM, Fuentes-Julián S, *et al*. Priming human adipose-derived mesenchymal stem cells for corneal surface regeneration. *J Cell Mol Med*. 2021;25(11):5124-5137. doi: 10.1111/jcmm.16501

17. Calonge M, Pérez I, Galindo S, *et al*. A proof-of-concept clinical trial using mesenchymal stem cells for the treatment of corneal epithelial stem cell deficiency. *Transl Res*. 2019;206:18-40. doi: 10.1016/j.trsl.2018.11.003

18. Cadenas-Martin M, Arnalich-Montiel F, Miguel MPD. Derivation of limbal stem cells from human adult mesenchymal stem cells for the treatment of limbal stem cell deficiency. *Int J Mol Sci*. 2023;24(3):2350. doi: 10.3390/ijms24032350

19. Edel MJ, Casellas HS, Osete JR, *et al*. An optimized method to produce human-induced pluripotent stem cell-derived limbal stem cells easily adaptable for clinical use. *Stem Cells Dev*. 2025;34(3-4):49-60. doi: 10.1089/scd.2024.0172

20. Bisevac J, Moe MC, Drolsum L, Kristianslund O, Petrovski G, Noer A. A novel technique of amniotic membrane preparation mimicking limbal epithelial crypts enhances the number of progenitor cells upon expansion. *Cells*. 2023;12(5):738. doi: 10.3390/cells12050738

21. Malhotra C, Jain AK. Human amniotic membrane transplantation: different modalities of its use in ophthalmology. *World J Transplant*. 2014;4(2):111. doi: 10.5500/wjt.v4.i2.111

22. Paolin A, Cogliati E, Trojan D, *et al*. Amniotic membranes in ophthalmology: long term data on transplantation outcomes. *Cell Tissue Bank*. 2016;17(1):51-58. doi: 10.1007/s10561-015-9520-y

23. Harkin DG, Foyn L, Bray LJ, Sutherland AJ, Li FJ, Cronin BG. Concise reviews: can mesenchymal stromal cells differentiate into corneal cells? A systematic review of published data. *Stem Cells*. 2015;33(3):785-791. doi: 10.1002/stem.1895

24. Nguyen KN, Bobba S, Richardson A, *et al*. Native and synthetic scaffolds for limbal epithelial stem cell transplantation. *Acta Biomater*. 2018;65:21-35. doi: 10.1016/j.actbio.2017.10.037

25. Tan G, Ioannou N, Mathew E, Tagalakis AD, Lamprou DA, Yu-Wai-Man C. 3D printing in ophthalmology: from

medical implants to personalised medicine. *Int J Pharm*. 2022;625:122094.
doi: 10.1016/j.ijpharm.2022.122094

26. Boularaoui S, Al Hussein G, Khan KA, Christoforou N, Stefanini C. An overview of extrusion-based bioprinting with a focus on induced shear stress and its effect on cell viability. *Bioprinting*. 2020;20:e00093.
doi: 10.1016/j.bprint.2020.e00093

27. Ng WL, Vyas C, Huang B, Yeong WY, Bartolo P. Advanced bioprinting strategies for fabrication of biomimetic tissues and organs. *Int J Extreme Manuf*. 2025; 7(6):062006.
doi: 10.1088/2631-7990/adeee0

28. De Miguel MP. European Patent Application No. 22382119.0. Published online 2022.

29. He Z, Forest F, Bernard A, *et al*. Cutting and decellularization of multiple corneal stromal lamellae for the bioengineering of endothelial grafts. *Invest Ophthalmol Vis Sci*. 2016;57(15):6639-6651.
doi: 10.1167/iovs.16-20256

30. Zuk PA, Zhu M, Ashjian P, *et al*. Human adipose tissue is a source of multipotent stem cells. *Mol Biol Cell*. 2002;13(12):4279-4295.
doi: 10.1091/mbc.E02-02-0105

31. Mikhailova A, Ilmarinen T, Uusitalo H, Skottman H. Small-molecule induction promotes corneal epithelial cell differentiation from human induced pluripotent stem cells. *Stem Cell Reports*. 2014;2(2):219-231.
doi: 10.1016/j.stemcr.2013.12.014

32. Casaroli-Marano RP, Martínez-Conesa EM, Nieto-Nicolau N, Arnalich-Montiel F, Fuentes-Julian S, De Miguel MP. Adipose derived stem cells (ADS) for ocular surface regeneration. *Invest Ophthalmol Vis Sci*. 2014; 55(13):5183.

33. Gerardo H, Lima A, Carvalho J, *et al*. Soft culture substrates favor stem-like cellular phenotype and facilitate reprogramming of human mesenchymal stem/stromal cells (hMSCs) through mechanotransduction. *Sci Rep*. 2019;9(1):9086.
doi: 10.1038/s41598-019-45352-3

34. Maddox JR, Ludlow KD, Li F, Niyibizi C. Breast and abdominal adipose multipotent mesenchymal stromal cells and stage-specific embryonic antigen 4 expression. *Cells Tissues Organs*. 2012;196(2):107-116.
doi: 10.1159/000331332

35. Guasti L, Prasongchean W, Kleftouris G, *et al*. High plasticity of pediatric adipose tissue-derived stem cells: too much for selective skeletogenic differentiation? *Stem Cells Transl Med*. 2012;1(5):384-395.
doi: 10.5966/sctm.2012-0009

36. Martínez-Conesa EM, Espel E, Reina M, Casaroli-Marano RP. Characterization of ocular surface epithelial and progenitor cell markers in human adipose stromal cells derived from lipoaspirates. *Invest Ophthalmol Vis Sci*. 2012;53(1):513-520.
doi: 10.1167/iovs.11-7550

37. Ahearne M, Masterton S. Donor dependent limbal derived stem cell response to fluidic shear stress. *Invest Ophthalmol Vis Sci*. 2024;65(7):4462-4462.

38. Di Iorio E, Barbaro V, Ruzza A, Ponzin D, Pellegrini G, De Luca M. *Isoforms of Np63 and the Migration of Ocular Limbal Cells in Human Corneal Regeneration*; 2005.
www.pnas.orgcgidoi10.1073pnas.0503437102

39. Collin J, Queen R, Zerti D, *et al*. A single cell atlas of human cornea that defines its development, limbal progenitor cells and their interactions with the immune cells. *Ocul Surf*. 2021;21:279-298.
doi: 10.1016/j.jtos.2021.03.010

40. Wang DY, Cheng CC, Kao MH, Hsueh YJ, Ma DHK, Chen JK. Regulation of limbal keratinocyte proliferation and differentiation by TAp63 and ΔNp63 transcription factors. *Invest Ophthalmol Vis Sci*. 2005;46(9):3102-3108.
doi: 10.1167/iovs.05-0051

41. Koster MI, Kim S, Mills AA, DeMayo FJ, Roop DR. p63 is the molecular switch for initiation of an epithelial stratification program. *Genes Dev*. 2004;18(2):126-131.
doi: 10.1101/gad.1165104

42. Verma S, Lin X, Coulson-Thomas VJ. The potential reversible transition between stem cells and transient-amplifying cells: the limbal epithelial stem cell perspective. *Cells*. 2024;13(9):748.
doi: 10.3390/cells13090748

43. Kalha S, Shrestha B, Sanz Navarro M, Jones KB, Klein OD, Michon F. Bmi1+ progenitor cell dynamics in murine cornea during homeostasis and wound healing. *Stem Cells*. 2018;36(4):562-573.
doi: 10.1002/stem.2767

44. Liang Q, Le Q, Wang L, *et al*. Cytokeratin 13 is a new biomarker for the diagnosis of limbal stem cell deficiency. *Cornea*. 2022;41(7):867-873.
doi: 10.1097/ICO.0000000000002903

45. Ramirez-Miranda A, Nakatsu MN, Zarei-Ghanavati S, Nguyen CV, Deng SX. Keratin 13 is a more specific marker of conjunctival epithelium than keratin 19. Mol Vis. 2011;17:1652-1661.
http://www.molvis.org/molvis/v17/a183

46. De Miguel MP, Cadenas-Martin M, Stokking M, Martin-Gonzalez AI. Biomedical application of MSCs in corneal regeneration and repair. *Int J Mol Sci*. 2025;26(2):695.
doi: 10.3390/ijms26020695

47. Dietrich-Ntoukas T, Hofmann-Rummelt C, Kruse FE, Schlötzer-Schrehardt U. *Comparative* analysis of the basement membrane composition of the human limbus epithelium and amniotic membrane epithelium. Cornea. 2012;31(5):564-569.
doi: 10.1097/ICO.0b013e3182254b78

48. Yazdanpanah G, Haq Z, Kang K, Jabbehdari S, Rosenblatt Ml, Djalilian AR. Strategies for reconstructing the limbal stem cell niche. *Ocular Surf*. 2019;17(2):230-240. doi: 10.1016/j.jtos.2019.01.002

49. Dong C, Lv Y. Application of collagen scaffold in tissue engineering: Recent advances and new perspectives. *Polymers (Basel)*. 2016;8(2):42. doi: 10.3390/polym8020042

50. Wang X, Majumdar S, Soiberman U, *et al*. Multifunctional synthetic Bowman's membrane-stromal biomimetic for corneal reconstruction. *Biomaterials*. 2020;241:119880. doi: 10.1016/j.biomaterials.2020.119880

51. Simpson FC, McTiernan CD, Islam MM, *et al*. Collagen analogs with phosphorylcholine are inflammation-suppressing scaffolds for corneal regeneration from alkali burns in mini-pigs. *Commun Biol*. 2021;4(1):608. doi: 10.1038/s42003-021-02108-y

52. Levis HJ, Daniels JT. Recreating the human limbal epithelial stem cell niche with bioengineered limbal crypts. *Curr Eye Res*. 2016;41(9):1153-1160. doi: 10.3109/02713683.2015.1095932

53. Zhang B, Xue Q, Li J, *et al*. 3D bioprinting for artificial cornea: challenges and perspectives. *Med Eng Phys*. 2019;71:68-78. doi: 10.1016/j.medengphy.2019.05.002

54. Bonnet C, Gonzalez S, Deng SX. Limbal stem cell therapy. *Curr Opin Ophthalmol*. 2024;35(4):309-314. doi: 10.1097/ICU.0000000000001061